MAJoRCom: A Dual-Function Radar Communication System Using Index Modulation

Tianyao Huang, Nir Shlezinger, Xingyu Xu, Yimin Liu, *Member, IEEE*, and Yonina C. Eldar, *Fellow, IEEE*

***Abstract*—Dual-function radar communication (DFRC) systems implement both sensing and communication using the same hardware. Such schemes are often more efficient in terms of size, power, and cost, over using distinct radar and communication systems. Since these functionalities share resources such as spectrum, power, and antennas, DFRC methods typically entail some degradation in both radar and communication performance. In this work we propose a DFRC scheme based on the carrier agile phased array radar (CAESAR), which combines frequency and spatial agility. The proposed DFRC system, referred to as multi-carrier agile joint radar communication (MAJoRCom), exploits the inherent spatial and spectral randomness of CAESAR to convey digital messages in the form of index modulation. The resulting communication scheme naturally coexists with the radar functionality, and thus does not come at the cost of reduced radar performance. We analyze the performance of MAJoRCom, quantifying its achievable bit rate. In addition, we develop a low complexity decoder and a codebook design approach, which simplify the recovery of the communicated bits. Our numerical results demonstrate that MAJoRCom is capable of achieving a bit rate which is comparable to utilizing independent communication modules without affecting the radar performance, and that our proposed low-complexity decoder allows the receiver to reliably recover the transmitted symbols with an affordable computational burden.**

***Index Terms*—Dual function radar communication, index modulation, frequency agile radar.**

I. Introduction

RECENT years have witnessed growing interest in dual-function radar communication (DFRC) systems. Many practical applications, including autonomous vehicles, commercial flight control, and military radar systems, implement both sensing as well as communications [3]–[7]. Jointly implementing radar and communication contributes to reducing the number of antennas [8], system size, weight, and power consumption [9], as well as alleviating concerns for electromagnetic compatibility (EMC) and spectrum congestion issues [3]. In one of the most common models for joint radar and communications, the DFRC system acts as the radar transceiver and communications transmitter simultaneously. This setup, which is considered henceforth, is commonly referred to as the *monostatic broadcast channel* [4, Sec. III-C]. In such scenarios, radar is regarded as the primary function and communications as the secondary one, sharing the high power and large bandwidth of the radar [10], [11].

Since DRFC systems implement both radar and communications using a single hardware device, these functionalities inherently share some of the system resources, such as spectrum, antennas, and power. To facilitate their coexistence, many different DFRC approaches have been proposed in the literature. In a single antenna radar or traditional phased array radar that transmits a single waveform, a common scheme is to utilize the communication signal as the radar probing waveform [12]. Such dual-function waveforms include phase modulation, as well as orthogonal frequency division multiplexing (OFDM) signaling [12], [13]. The design of such waveforms to fit a given beam pattern was studied in [14]. However, this approach tends to come at the cost of reducing radar performance compared to using dedicated radar signals [11], [15]. Furthermore, transmitting non-constant modulus communication waveforms may result in low power efficiency when using practical non-linear amplifiers.

Another common DFRC approach is to utilize different signals for radar and communications, designing the functionalities to co-exist by mitigating their cross interference. Multiple-input multiple-output (MIMO) radar systems in which a subset of the antenna array is allocated to radar and the rest to communications were studied in [15], along with the setup in which both functionalities utilize all the antennas. Methods for treating the effect of spectrally interfering separate radar and communication systems were studied in [16], [17], while [18] analyzed the effect of radar interference on communication systems. Frequency allocation among radar and communications was considered in [19]. Coexistence in MIMO DFRC systems can be realized using beamforming, namely, by generating multiple beams with different waveforms towards radar targets and communication users at diverse directions [20]–[22]. The work [23] proposed a scheme based on generalized spatial modulation (GSM) [24], [25], in which some of the information bits are conveyed in the selection of the antennas utilized for communication. The

Manuscript received September 9, 2019; revised March 2, 2020 and April 19, 2020; accepted May 5, 2020. Date of publication May 14, 2020; date of current version June 16, 2020. The associate editor coordinating the review of this manuscript and approving it for publication was Dr. Fabiola Colone. This work was supported in part by the National Natural Science Foundation of China under Grants 61801258 and 61571260, in part by the European Union's Horizon 2020 research and innovation program under Grant 646804-ERC-COG-BNYQ, and in part by the Air Force Office of Scientific Research under Grant FA9550-18-1-0208. This article was presented in part at the IEEE International Workshop on Signal Processing Advances in Wireless Communications, Cannes, France, 2019 and in part at the 45th International Conference on Acoustics, Speech, and Signal Processing, 2020. *(Corresponding author: Yimin Liu.)*

Tianyao Huang, Xingyu Xu, and Yimin Liu are with the Department of Electrical Engineering, Tsinghua University, Beijing 100084, China (e-mail: huangtianyao@tsinghua.edu.cn; xy-xu15@mails.tsinghua.edu.cn; yiminliu@tsinghua.edu.cn).

Nir Shlezinger and Yonina C. Eldar are with the Faculty of Math and CS, Weizmann Institute of Science, Rehovot 7610001, Israel (e-mail: nirshlezinger1@gmail.com; yonina.eldar@weizmann.ac.il).

Digital Object Identifier 10.1109/TSP.2020.2994394

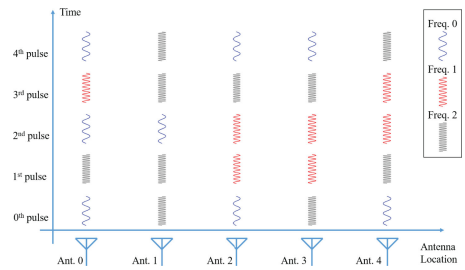

Fig. 1. Transmission example of CAESAR [33]. In every pulse of this example, two out of three carrier frequencies are emitted by different sub-arrays. For example, frequency 0 and 2 are selected in the 0-th pulse and are sent by antennas 0, 2, 4 and antennas 1, 3, respectively. FAR is a special case of CAESAR, with only one out of three frequencies sent in each pulse.

drawback of these previous DFRC methods, particularly when radar is the primary functionality, is that communication interferes with the radar, either via spectral interference, power sharing, or by reducing the number of available antennas. This results in an inherent tradeoff between radar and communication performance [26], [27].

An alternative DFRC strategy is to incorporate communication functionality into existing radar schemes, allowing the radar to operate without notably affecting its performance when it conveys digital messages. For example, the works [28], [29] proposed embedding communication bits in the selection of the chirp rates using wideband linear frequency modulation waveforms. Another common radar technique which can be extended into a DFRC system is MIMO radar, in which each antenna element transmits a different orthogonal waveform, enhancing the flexibility in transmit beam pattern design [30]. The resulting waveform diversity can be exploited to embed information bits into the transmitted signal with minimal effect on the radar performance. For example, the information bits can be conveyed in the sidelobe levels [31] or via frequency hopping codes [32]. The recent work [11] selected a sparse array out of the complete array antenna, each antenna unit transmitting a different predefined orthogonal waveform. The selection of orthogonal waveforms and permutation of the antennas were studied as methods for embedding information bits, resulting in a waveform and antenna index modulation scheme. However, the usage of sparse arrays reduces transmit power and antenna gain, thus degrading the radar target detection performance. Since radar returns of all orthogonal waveforms are received by each antenna element, MIMO radar receivers usually operate at a large bandwidth, resulting in high complexity in hardware and computing. Consequently, these DFRC approaches may be difficult to implement in practice and cannot be applied in many existing radar architectures.

In our previous work [33] we proposed CAESAR, which is a radar capable of approaching wideband performance while utilizing narrowband signals. This improved performance is achieved by combining the concept of frequency agile radar (FAR), in which the carrier frequencies vary from pulse to pulse [34], with *spatial agility*. In particular, CAESAR randomly chooses multiple frequencies simultaneously in a single pulse, and then selects a set of antennas for each chosen frequency such that each set of antennas uses a different frequency as depicted in Fig. 1. In the reception stage, each array element acquires the radar returns at the same single frequency as in the transmitting stage, which reduces hardware complexity in comparison with MIMO radar architectures. The resulting radar scheme has excellent electronic counter-countermeasures (ECCM) and EMC performance; it supports spectrum sharing in congested electromagnetic environments; and its radar performance is comparable to that of costly wideband radar [33]. In addition to the aforementioned advantages, the inherent spectral and spatial randomness of CAESAR can be utilized to convey information using index modulation methods, in which the indices of the building blocks (e.g., frequencies and/or antennas) are used to convey additional information bits [25], [35], [36], *without degrading radar performance*. The resulting MAJoRCom system is the focus of the current work.

Here, we propose MAJoRCom: a DFRC system equipped with a phased array antenna, in which radar is the primary user and is based on CAESAR. We show how CAESAR is capable of conveying information to a remote receiver using index modulation. MAJoRCom utilizes the selections of carrier frequencies and their allocation among the antenna elements of CAESAR to convey digital information in a combination of frequency index modulation [37] and spatial index modulation [35]. Unlike previously proposed DFRC systems [12]–[16], [19], [23], which use dedicated independent waveforms and/or antennas for communication, in MAJoRCom the ability to convey information is an inherent byproduct of the radar scheme. Consequently, communication transmission is naturally obtained from the radar design, and both functionalities coexist without cross interference.

We analyze the communication performance of MAJoRCom. Since the communication functionality does not interfere with the radar subsystem, the radar performance of MAJoRCom is the same as CAESAR, and was studied in our previous work [33]. Here, we first detail the scheme for embedding digital communication messages into the radar transmission. We then characterize the achievable rate of MAJoRCom, and show that the maximal number of bits which can be conveyed in each pulse grows linearly with the number of transmit antennas and logarithmically with the number of available carrier frequencies. To overcome the increased computational complexity associated with index modulation decoding [38], we propose a low complexity communication receiver structure and design a permutation codebook to facilitate decoding. MAJoRCom is evaluated in a numerical study, demonstrating its capability to achieve comparable communication rates with DFRC systems using antennas that are dedicated for communication only, without affecting the radar performance and resources.

Our main contributions are summarized as follows:

- We propose MAJoRCom which is a DFRC system that arises from CAESAR. The communication scheme of MAJoRCom exploits the agile profile of the radar waveforms used by CAESAR to convey its message via frequency and spatial index modulation. These forms of index modulation, commonly studied in the communication literature as methods for boosting energy and spectral efficiency of digital modulations [25], [35], [37], use the selections of frequencies and the corresponding antenna elements to embed information, without requiring the transmitter to have channel state information (CSI). This integration of index modulation based communications and agile radar yields a

dual function system in which the ability to communication messages does not affect the power and waveform of the radar functionality.
- We analyze the achievable information rate of MAJoRCom. In particular, we show that the maximal number of bits which can embedded into each pulse, representing an upper bound on the information rate which is achievable in high signal-to-noise ratio (SNR), grows logarithmically with the number of carrier frequencies. This indicates that increasing the agility of the radar also contributes to its achievable rate.
- We propose a low complexity decoder, which achieves comparable bit error rate (BER) performance as the optimal decoder. Codeword design approaches are also proposed to further facilitate decoding, at the cost of reducing the information rate. Both proposed complexity reduction methods are specifically tailored for the unique signaling method of MAJoRCom, which combines index modulation and narrowband radar waveforms.

The main advantage of MAJoRCom over previously proposed DFRC systems, e.g., [12]–[15], [19], [23], is that it provides the ability to communicate without affecting the radar subsystem, while supporting the usage of simple narrowband transceivers.

The rest of paper is organized as follows. Section II reviews CAESAR and introduces MAJoRCom, which applies frequency selection and spatial permutation to convey digital messages. Section III is devoted to communication analysis, while Section IV introduces low-complexity receiver and codebook design methods. Numerical results are provided in Section V, followed by concluding remarks in Section VI.

Throughout the paper we use the following notation: The sets $\mathbb{C}$, $\mathbb{R}$ and $\mathbb{Z}$ are the complex, real and integer numbers, respectively. We use $|\cdot|$ for the magnitude or cardinality of a scalar value or a set, respectively. We denote by $\lfloor x \rfloor$ the largest integer less than or equal to $x \in \mathbb{R}$. Uppercase and lowercase boldface letters are used for matrices and vectors, respectively. The m,n-th (n-th) element of matrix $\boldsymbol{A}$ (vector $\boldsymbol{a}$) is written as $[\boldsymbol{A}]_{m,n}$ ($[\boldsymbol{a}]_n$). We use $\mathbf{0}/\mathbf{1}_{n\times m}$ to denote a $n \times m$ dimensional matrix with all entries being 0/1. The complex conjugate operator, transpose operator, and the complex conjugate-transpose operator are denoted by $(\cdot)^*$, $(\cdot)^T$, and $(\cdot)^H$. We use $\|\cdot\|_p$ as the ℓ_p norm of an argument, and $\mathbb{E}[\cdot]$ is the stochastic expectation.

II. MAJoRCom System Model

In this work, we propose MAJoRCom, which jointly implements radar as well as the ability of communicating information to a remote receiver. Radar is considered to be the primary user, and is based on the recently proposed CAESAR system [33]. The communication method is integrated into CAESAR to avoid coexistence issues. In order to formulate MAJoRCom, we first review CAESAR in Subsection II-A, after which we present its extension to a DFRC system in Subsection II-B.

A. Carrier Agile Phased Array Radar

CAESAR is a recently proposed radar scheme [33] which extends the concept of FAR [34]. This technique was shown to enhance the ECCM and EMC radar measures as well as achieve improved target reconstruction performance while avoiding costly instantaneous wideband components [33]. Broadly speaking, CAESAR randomly changes the carrier frequencies from pulse to pulse, maintaining the frequency agility of FAR, while allocating these frequencies among its antenna elements in a random fashion, introducing spatial agility. An illustration of this scheme is depicted in Fig. 1.

To properly formulate CAESAR, consider a radar system equipped with L_{R} antenna elements, uniformly spaced with distance d between two adjacent elements. Let $\mathcal{F}$ be the set containing the available carrier frequencies of cardinality M, given by

$$\mathcal{F} := \{f_c + m\Delta f | m \in \mathcal{M}\}, \tag{1}$$

where $\mathcal{M} := \{0, 1, \ldots, M-1\}$, f_c is the initial carrier frequency, and Δf is the frequency step. Let N be the number of radar pulses transmitted in each coherent processing interval. Radar pulses are repeatedly transmitted, starting from time instance nT_r to $nT_r + T_p$, $n \in \{0, 1, \ldots, N-1\} := \mathcal{N}$, where T_r and T_p are the pulse repetition interval and duration, respectively, $T_r > T_p$.

In the n-th pulse, CAESAR randomly selects a set of carrier frequencies $\mathcal{F}_n$ from $\mathcal{F}$, $\mathcal{F}_n \subset \mathcal{F}$. We assume that the cardinality of $\mathcal{F}_n$ is constant, i.e., $|\mathcal{F}_n| = K$ for each $n \in \mathcal{N}$, and write the elements of this set as $\mathcal{F}_n = \{\Omega_{n,0}, \ldots, \Omega_{n,K-1}\}$. A subarray is allocated for each frequency, such that all the antenna array elements are utilized for transmission and each element transmits at a single carrier frequency. Denote by $f_{n,l} \in \mathcal{F}_n$ the frequency used by the l-th antenna array element, i.e., if $\Omega_{n,k}$ is the frequency used by the l-th element then $f_{n,l} = \Omega_{n,k}$. The waveform sent from the lth element for the n-th pulse is expressed as $\phi(f_{n,l}, t - nT_r)$, where $\phi(f,t) := \mathrm{rect}(t/T_p)e^{j2\pi ft}$. In order to direct the antenna beam pointing towards a desired angle θ, the signal transmitted by each antenna is weighted by the function $w_l(\theta, f_{n,l}) \in \mathbb{C}$, which is set to [39]

$$w_l(\theta, f_{n,l}) = e^{j2\pi f_{n,l} l d \sin\theta/c}, \tag{2}$$

where c denotes the speed of light. Here, when the relative bandwidth is small, i.e., $M\Delta f/f_c \ll 1$, the weight $w_l(\theta, f_{n,l})$ may be approximated by $e^{j2\pi f_c l d \sin\theta/c}$, which depends only on the initial frequency f_c. The transmission of the l-th array element can thus be written as

$$[\boldsymbol{x}(n,t)]_l = w_l(\theta, f_{n,l})\phi(f_{n,l}, t - nT_r). \tag{3}$$

The vector $\boldsymbol{x}(n,t) \in \mathbb{C}^{L_{\mathrm{R}}}$ in (3) denotes the transmission vector of the full array for the n-th pulse at time instance t. An illustration of such a transmission is depicted in Fig. 1. The transmitted signal (3) can also be expressed by grouping the array elements which use the same frequency $\Omega_{n,k}$, $k = 0, \ldots, K-1$. Let $\boldsymbol{x}_k(n,t) \in \mathbb{C}^{L_{\mathrm{R}}}$ represent the portion of $\boldsymbol{x}(n,t)$, which utilizes $\Omega_{n,k}$, i.e., $\boldsymbol{x}(n,t) = \sum_{k=0}^{K-1} \boldsymbol{x}_k(n,t)$. The transmitted signal may now be written as

$$\boldsymbol{x}(n,t) := \sum_{k=0}^{K-1} \boldsymbol{P}(n,k)\boldsymbol{w}(\theta, \Omega_{n,k})\,\phi(\Omega_{n,k}, t - nT_r). \tag{4}$$

Here, $\boldsymbol{w}(\theta, f)$ is an $L_R \times 1$ vector whose l-th entry is $w_l(\theta, f)$ defined in (2). The diagonal matrix $\boldsymbol{P}(n,k) \in \{0,1\}^{L_{\mathrm{R}} \times L_{\mathrm{R}}}$ is determined by its diagonal vector $\boldsymbol{p}(n,k) \in \{0,1\}^{L_{\mathrm{R}}}$, whose l-th entry is 1 if the corresponding array element uses $\Omega_{n,k}$ and 0 otherwise, i.e., $[\boldsymbol{P}(n,k)]_{l,l} = [\boldsymbol{p}(n,k)]_l = 1$ when $[\boldsymbol{x}_k(n,t)]_l \neq 0$.

In the reception stage of the n-th pulse, i.e., $nT_r + T_p < t < (n+1)T_r$, the l-th antenna element only receives radar returns at

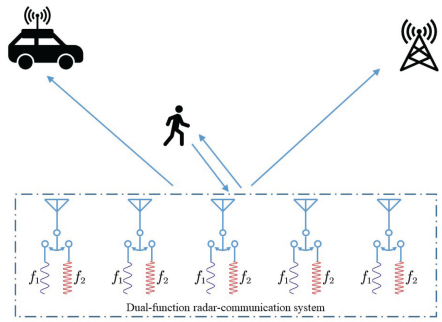

Fig. 2. A phased array DFRC system, which can detect targets (e.g., the pedestrian) and send communication symbols to remote receivers. Each array element independently selects the carrier frequency, e.g. from f_1 and f_2.

frequency $f_{n,l}$, and abandons returns at other frequencies, facilitating the usage of narrowband radar receiver and simplifying the hardware requirements. Our proposed extension of CAESAR to a DFRC system, detailed in the following subsection, exploits the transmitted signal model (4), and does not depend on the observed radar returns and processing strategy. The readers are referred to [33] for a detailed description of the received radar signal model, target recovery methods, and radar performance analysis of CAESAR.

B. Information Embedding Approach

The inherent randomness in the selection of carrier frequencies and their allocation among the transmit antennas can be exploited to convey information in the form of index and permutation modulations. Index modulation refers to the embedding of information bits through indices of certain parameters involved in the transmission [35], most commonly the subcarrier index in OFDM modulation, i.e., frequency index modulation [37], or the antenna selection in MIMO communications, namely, spatial modulation [24], [25]. CAESAR randomly selects an index corresponding to a set of carrier frequencies, and permutes the selected frequencies and the corresponding antenna elements, which can either be treated as an index of a specific permutation, or as a permutation modulation codeword [40]. By doing so, CAESAR realizes a DFRC system, as illustrated in Fig. 2 for the setting of $|\mathcal{F}| = M = 2$. Consequently, a natural extension of CAESAR is to utilize this randomness to convey information to a remote receiver, thus realizing digital communications without affecting the radar functionality.

The proposed information embedding method is applied identically on each pulse, where transmitting more pulses results in more bits being conveyed to the receiver. Consequently, in order to formulate the embedding method, we only consider a single pulse in this section. Accordingly, we simplify our notations as follows: $\boldsymbol{P}_k := \boldsymbol{P}(n,k)$, $\boldsymbol{p}_k := \boldsymbol{p}(n,k)$, $\boldsymbol{x}(t) := \boldsymbol{x}(n,t)$, $\boldsymbol{x}_k(t) := \boldsymbol{x}_k(n,t)$, and $\boldsymbol{w}_k := \boldsymbol{w}(\theta, \Omega_{n,k})$.

Before transmitting the dual function waveform, CAESAR first selects frequencies and then allocates array elements to each frequency. The randomness of digital communication messages is utilized to convey information in the selection of the frequencies subset and in the allocation of the subset among the transmit antennas. We propose to exploit this fact to generate two sets of codewords, combined into a hybrid modulation strategy, as discussed next.

1) Frequency Index Modulation: Recall that at each transmission, K out of M frequencies in $\mathcal{F}$ are used. The set of possible frequency selections at each pulse is denoted by

$$\mho := \left\{ \mathcal{F}^{(i)} \,\middle|\, \left|\mathcal{F}^{(i)}\right| = K, \mathcal{F}^{(i)} \subset \mathcal{F}, i = 0, 1, 2, \dots \right\}, \quad (5)$$

where the superscript (i) stands for the i-th codeword in the set $\mho$. The number of possible frequency selections is thus

$$|\mho| = \binom{M}{K} = \frac{M!}{K!(M-K)!}. \quad (6)$$

2) Spatial Index Modulation: Once the carrier frequencies are selected, each antenna element uses a single frequency to transmit its monotone waveform. To mathematically formulate this allocation, we define $L_K := L_{\mathrm{R}}/K \geq 1$, which is assumed to be an integer, and allow each frequency to be utilized by exactly L_K antenna elements[1] assigned to the selected K frequencies. The diagonal selection matrices $\{\boldsymbol{P}_k\}$ uniquely describe the allocation of antenna elements. We note that $\mathrm{tr}(\boldsymbol{P}_k) = L_K$, as exactly L_K antennas use the k-th frequency, and $\sum_{k=0}^{K-1} \boldsymbol{P}_k = \boldsymbol{I}_{L_{\mathrm{R}}}$, indicating that all the antenna elements are utilized. Let $\mathcal{P}$ denote the set of all possible allocation patterns, given by

$$\mathcal{P} := \left\{ \boldsymbol{P}_0^{(i)}, \dots, \boldsymbol{P}_{K-1}^{(i)} \,\middle|\, i = 0, 1, \dots \right\}, \quad (7)$$

where the superscript (i) stands for the i-th allocation pattern. Note that the number of patterns is

$$|\mathcal{P}| = \frac{L_{\mathrm{R}}!}{(L_K!)^K}. \quad (8)$$

As an example, consider a MAJoRCom system equipped with $L_{\mathrm{R}} = 4$ antennas, transmitting $K = 2$ frequencies in each pulse, namely, each frequency is utilized by $L_K = 2$ antennas. In this case, the number of codewords which can be conveyed by this spatial permutation is $\frac{4!}{(2!)^2} = 6$. The first three possible selection patterns are:

$$\begin{aligned} \boldsymbol{p}_0^{(0)} &= [1,1,0,0]^T, \boldsymbol{p}_1^{(0)} = [0,0,1,1]^T, \\ \boldsymbol{p}_0^{(1)} &= [1,0,1,0]^T, \boldsymbol{p}_1^{(1)} = [0,1,0,1]^T, \\ \boldsymbol{p}_0^{(2)} &= [1,0,0,1]^T, \boldsymbol{p}_1^{(2)} = [0,1,1,0]^T. \end{aligned} \quad (9)$$

The remaining three matrices are obtained by interchanging the subscripts, e.g., by setting $\boldsymbol{p}_0^{(3)} = \boldsymbol{p}_1^{(0)}$, $\boldsymbol{p}_1^{(3)} = \boldsymbol{p}_0^{(0)}$.

3) Hybrid Modulation: Combining frequency and antenna selection yields a hybrid frequency and spatial index modulation scheme, in which the total number of codewords is

$$|\mho|\,|\mathcal{P}| = \frac{M!}{K!(M-K)!} \frac{L_{\mathrm{R}}!}{(L_K!)^K}. \quad (10)$$

It follows from (10) that the maximum number of bits which can be conveyed in each pulse is

$$\log_2 |\mho| + \log_2 |\mathcal{P}| = \log_2 \frac{M!}{K!(M-K)!} + \log_2 \frac{L_{\mathrm{R}}!}{(L_K!)^K}. \quad (11)$$

[1]The assumption that L_R/K is an integer is used only to facilitate the formulation of the permutation technique. Clearly, the proposed spatial index modulation can be extended to the case that L_{R} is not an integer multiple of K and that antennas are unevenly allocated by adapting the above arguments.

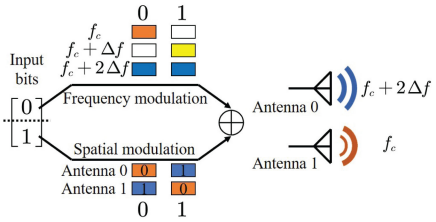

Fig. 3. Hybrid frequency and spatial index signaling of MAJoRCom.

Using Stirling's formula $\log_2 n! \approx n\log_2 n - n\log_2 e$, the number of bits (11) can be approximated as

$$\log_2|\mathcal{U}|+\log_2|\mathcal{P}| \approx \log_2\left(\frac{M^M}{(M-K)^{M-K}K^K}\right)+L_{\mathrm{R}}\log_2 K$$
$$\approx K\log_2 M + L_{\mathrm{R}}\log_2 K. \quad (12)$$

This approximation holds for a large number of antennas L_{R} and a large number of frequencies M such that $L_{\mathrm{R}} \gg K$ and $M \gg K$. It follows from (12) that the number of bits grows linearly with L_{R} and logarithmically with M, indicating the theoretical benefits of utilizing MAJoRCom with large-scale antenna arrays where M is large.

The proposed information embedding is carried out as follows: At each pulse, the input bits are divided into two sets. The first set of bits is used for selecting the frequencies $\mathcal{F}$ from $\mathcal{U}$, while the remaining bits determine the pattern of antenna allocation from $\mathcal{P}$. An example of this scheme is depicted in Fig. 3. This method bears some similarity to generalized space-frequency index modulation proposed in [41]. In particular, both techniques convey information in the selection of the carrier frequencies as well as in the form of the signal transmitted by each antenna element. Nonetheless, while [41] transmits an OFDM signal consisting of multiple subcarriers from a subset of the complete antenna array, MAJoRCom utilizes a single carrier frequency at each transmit antenna and transmits a radar waveform using all the available antennas. Consequently, our approach transmits constant modulus monotone signals, and utilizes the complete antenna array, maximizing the radar power and aperture. For the radar function, use of the complete antenna array is beneficial, because it leads to a more directional beam and higher antenna gain, which is important for target detection, especially in tracking mode [42]. In contrast, [41] embeds information in the selection of active antennas, leading to incomplete antenna aperture and reduction of radar performance.

MAJoRCom does not require the DFRC system to have CSI, namely, no a-priori knowledge of the channel to the receiver is required in order to embed the information, as opposed to, e.g., spatial beamforming-based DFRC systems [21], [43]. Such knowledge is only needed at the receiver to facilitate decoding, as discussed in the following section. Furthermore, while we assume that the radar waveform $\phi(f,t) := \mathrm{rect}(t/T_p)e^{j2\pi ft}$ does not convey informative bits, MAJoRCom can clearly be extended to embed data into the waveform. For example, by utilizing GSM [24], [25], the proposed hybrid frequency and spatial modulation can potentially increase the communication rate. However, such a modification would come at the cost of some degradation in radar performance as the radar depends on the waveform and available resources.

A related DFRC scheme is that proposed in [11], which is based on MIMO radar with sparse arrays, in which bits are embedded in the orthogonal waveform and sparse array antenna index. The differences between [11] and our proposed MAJoRCom are not only in the radar schemes, as discussed in the introduction, but also in the information embedding method. MAJoRCom allocates a sub-array antenna for each selected carrier frequency, while the system proposed in [11] chooses a single antenna unit for each orthogonal waveform, resulting in different signaling strategies and lower data rates compared to MAJoRCom.

The fact that the radar subsystem of MAJoRCom implements CAESAR without affecting its radar performance follows from the underlying assumption that the communication codewords are random and equally distributed. Under this assumption, the available carrier frequencies are used with equal probability as in CAESAR [33], leading to a random sensing matrix for range-Doppler reconstruction, which guarantees the range-Doppler recovery performance, see [33, Sec. IV]. The randomly varied array allocation pattern results in a spatial beam pattern with moderate side lobe levels, as numerically demonstrated in our simulation study in Section V.

While equiprobale symbols are a common model for transmitted messages in digital communications, when this model does not hold, the radar performance of MAJoRCom is expected to deviate from that of CAESAR. To see this, consider the extreme case in which, instead of having the codewords randomized in a uniform fashion, the same codeword is transmitted repeatedly in a coherence processing interval, i.e., the same carrier frequencies and array allocation pattern are used. Such non-random allocation clearly affects the range-Doppler recovery performance as well as the resulting beam pattern. Particularly, the sensing matrix for range-Doppler reconstruction used for target recovery in [33] becomes a deterministic matrix. Furthermore, since only a small portion of available carrier frequencies are used for probing, the sub-matrix of the sensing matrix corresponding to a specific Doppler parameter becomes rank deficient. Consequently, CAESAR target detection is no longer guaranteed to stably recover the high range resolution parameters of targets, although the reconstruction of Doppler parameters is still possible, as we numerically demonstrate in Section V. The resulting lack of spatial agility also affects the beam pattern, and may widen the main lobe or increase the side lobe levels, depending on the specific array allocation pattern.

III. Communication Performance Analysis

We now analyze the communication performance of MAJoRCom in terms of achievable rate. To that aim, we first derive the received communication signal model in Subsection III-A, and then characterize the achievable rate in Subsection III-B. This analysis allows us to numerically evaluate the communication capabilities of MAJoRCom in Section V, where we demonstrate that its achievable rate is comparable to using dedicated communication waveforms, without affecting radar performance.

A. Received Communication Signal Model

To model the signal observed by the remote communication receiver, let L_{C} denote the number of receiver antennas, and consider a memoryless additive white Gaussian noise channel.

The channel output observed by the receiver, $\boldsymbol{y}_{\mathrm{C}}(t) \in \mathbb{C}^{L_{\mathrm{C}}}$, is given by

$$\boldsymbol{y}_{\mathrm{C}}(t) = \sum_{k=0}^{K-1} \boldsymbol{H}\boldsymbol{x}_k(t) + \boldsymbol{n}_{\mathrm{C}}(t), \tag{13}$$

where $\boldsymbol{n}_{\mathrm{C}}(t) \in \mathbb{C}^{L_{\mathrm{C}}}$ is the additive Gaussian noise signal and $\boldsymbol{H} \in \mathbb{C}^{L_{\mathrm{C}} \times L_{\mathrm{R}}}$ is the channel matrix representing the complex-valued fluctuations between the MAJoRCom system and the remote receiver. The proposed model can be extended to account for frequency selective channels by using bandlimited waveforms whose bandwidth is no larger than the channel coherence bandwidth. In this case, the matrix $\boldsymbol{H}$ in (13) is replaced with the frequency index dependent matrix $\boldsymbol{H}_k$.

After down-conversion by $e^{-j2\pi f_c t}$, the receiver samples the signal at time instances iT_s, where T_s is the sampling interval, and $i = 0, 1, \ldots, \lfloor T_p/T_s \rfloor$, resulting in $L_T := \lfloor T_p/T_s \rfloor + 1$ outputs per pulse. We assume that the receiver observes the complete frequency range $\mathcal{F}$, and applies Nyquist sampling rate of the entire band, $T_s = \frac{1}{M\Delta f}$. We refer to [44], [45] and references therein for sub-sampling approaches. By letting $\boldsymbol{Y}_{\mathrm{C}}, \boldsymbol{N}_{\mathrm{C}} \in \mathbb{C}^{L_{\mathrm{C}} \times L_T}$ denote the sampled channel output and noise corresponding to a single pulse in matrix form, respectively, it follows from the transmit signal model (4) that

$$\boldsymbol{Y}_{\mathrm{C}} = \sum_{k=0}^{K-1} \boldsymbol{H}\boldsymbol{P}_k\boldsymbol{w}_k\boldsymbol{\psi}_{c_k}^T + \boldsymbol{N}_{\mathrm{C}}. \tag{14}$$

In (14), we define $c_k := (\Omega_{n,k} - f_c)/\Delta f \in \mathcal{M}$ as the frequency codeword corresponding to $\Omega_{n,k}$, and $\boldsymbol{\psi}_{c_k} := [1, e^{j2\pi c_k \Delta f T_s \cdot 1}, \ldots, e^{j2\pi c_k \Delta f T_s \cdot (L_T-1)}]^T \in \mathbb{C}^{L_T}$ as the baseband signal corresponding to the frequency codeword c_k.

We assume that the receiver knows the number of frequencies K, the pointing direction of radar θ, CSI, i.e., knowledge of the channel matrix $\boldsymbol{H}$, and the distribution of the additive noise. Therefore, the steering vectors $\{\boldsymbol{w}_k\}$ are known once the frequencies are estimated. When the relative bandwidth is small, we also assume that $\{\boldsymbol{w}_k\}$ are known, since these weights are approximately determined by the a priori known initial frequency f_c. We note that such CSI is only required at the receiver side. The fact that for a fixed frequency-antenna allocation, the transmitted waveform is deterministic, can be utilized to facilitate channel acquisition in a pilot-aided fashion when $\boldsymbol{H}$ has to estimated. We leave the analysis of channel estimation and its effect on the system performance, as well as the design of frequency-antenna allocation pilot sequences for future investigation, and focus here on the case where $\boldsymbol{H}$ is known at the receiver. Under the above signal model, we next study the achievable rate.

B. Achievable Rate Analysis

In order to evaluate the proposed communication system, we characterize its achievable rate, namely, the maximal number of bits which can be reliably conveyed to the receiver at a given noise level in each pulse. To facilitate the analysis, we assume that each discrete-time channel output represents a single pulse, i.e., $L_T = 1$. The following analysis can be extended to any positive integer value of L_T. Under this model, for each pulse, the input-output relationship of the communication channel (14) is given by

$$\boldsymbol{y}_{\mathrm{C}} = \boldsymbol{H}\boldsymbol{x} + \boldsymbol{n}_{\mathrm{C}}, \tag{15}$$

where $\boldsymbol{x} = \sum_{k=0}^{K-1} \boldsymbol{P}_k\boldsymbol{w}_k$, and $\boldsymbol{n}_{\mathrm{C}}$ is additive white Gaussian noise with covariance $\sigma^2\boldsymbol{I}_{L_{\mathrm{C}}}$, independent of $\boldsymbol{x}$. Previous works which characterized bounds on the achievable rates of index modulation techniques, e.g., [38], [46], assumed that the channel input includes a digitally modulated symbol whose parameters are exploited to convey additional information via index modulation. Here, the primary user is the radar functionality, and the channel input $\boldsymbol{x}$ in (15) is a radar waveform. The information bits are embedded in $\boldsymbol{x} = \sum_{k=0}^{K-1} \boldsymbol{P}_k\boldsymbol{w}_k$, via the set of carrier frequencies, encapsulated in $\{\boldsymbol{w}_k\}$, and their antenna allocation, modeled via $\{\boldsymbol{P}_k\}$. The following achievable rate study is thus specifically tailored for the statistical characterization of $\boldsymbol{x}$ which arises in MAJoRCom.

Based on the transmission scheme detailed in Section II, we define a set $\mathcal{X} \subset \mathbb{C}^{L_{\mathrm{R}}}$ that contains all the possible transmitted signal vectors $\boldsymbol{x}$, whose carnality is $|\mathcal{X}| = \frac{M!}{K!(M-K)!}\frac{L_R!}{(L_K!)^K}$. Assuming that the codewords are equally distributed, it holds that $\boldsymbol{x}$ is uniformly distributed over $\mathcal{X}$. Consequently, the channel output $\boldsymbol{y}_{\mathrm{C}}$ obeys a Gaussian mixture (GM) distribution with equal priors. Let $f_{G_{L_{\mathrm{C}}}}(\boldsymbol{u}; \boldsymbol{m}, \boldsymbol{C})$ denote the probability density function (PDF) of an $L_{\mathrm{C}} \times 1$ proper-complex Gaussian vector with mean $\boldsymbol{m} \in \mathbb{C}^{L_{\mathrm{C}}}$ and covariance matrix $\boldsymbol{C} \in \mathbb{C}^{L_{\mathrm{C}} \times L_{\mathrm{C}}}$, where $\boldsymbol{u}$ is the realization of the random vector. Then, the PDF of $\boldsymbol{y}_{\mathrm{C}}$ is

$$f_{\boldsymbol{y}_{\mathrm{C}}}(\boldsymbol{u}) = \frac{1}{|\mathcal{X}|} \sum_{\boldsymbol{x}^{(i)} \in \mathcal{X}} f_{G_{L_{\mathrm{C}}}}\left(\boldsymbol{u}; \boldsymbol{H}\boldsymbol{x}^{(i)}, \sigma^2\boldsymbol{I}_{L_{\mathrm{C}}}\right). \tag{16}$$

Using the input-output relationship of the channel, we now characterize the achievable rate. Let $I(\cdot;\cdot)$ and $h(\cdot)$ denote the mutual information and differential entropy, respectively. Since the channel in (15) is memoryless, its achievable rate is given by the single letter characterization [47]

$$\begin{aligned} R_{\mathrm{C}} &= I(\boldsymbol{x}; \boldsymbol{y}_{\mathrm{C}}) = h(\boldsymbol{y}_{\mathrm{C}}) - h(\boldsymbol{y}_{\mathrm{C}}|\,\boldsymbol{x}) \\ &= h(\boldsymbol{y}_{\mathrm{C}}) - h(\boldsymbol{n}_{\mathrm{C}}) \qquad (17) \\ &= h(\boldsymbol{y}_{\mathrm{C}}) - L_{\mathrm{C}} \cdot \log_2\left(\pi \cdot e \cdot \sigma^2\right), \qquad (18) \end{aligned}$$

where (17) holds since $\boldsymbol{x}$ is independent of $\boldsymbol{n}_{\mathrm{C}}$, and (18) is the differential entropy of proper-complex Gaussian vectors.

In order to evaluate (18), one has to compute the differential entropy of the GM random vector $\boldsymbol{y}_{\mathrm{C}}$. While there is no closed-form analytic expression for the differential entropy of GM random vectors [48], a lower bound on the achievable rate can be obtained, as stated in the following proposition:

Proposition 1: The achievable rate of the proposed communication scheme is lower bounded by

$$R_{\mathrm{C}} \geq -\frac{1}{|\mathcal{X}|} \sum_{\boldsymbol{x}^{(i)} \in \mathcal{X}} \log_2 f_{\boldsymbol{y}_{\mathrm{C}}}\left(\boldsymbol{H}\boldsymbol{x}^{(i)}\right) - L_{\mathrm{C}} \cdot \log_2\left(\pi \cdot e \cdot \sigma^2\right),$$

where $f_{\boldsymbol{y}_{\mathrm{C}}}(\cdot)$ is given in (16).

Proof: The proposition follows from lower bounding $h(\boldsymbol{y}_c)$ using [48, Thm. 2]. ■

A trivial upper bound on R_{C} is obtained by noting that $\boldsymbol{x}$ is uniformly distributed over the discrete set $\mathcal{X}$, thus,

$$R_{\mathrm{C}} \leq h(\boldsymbol{x}) = \log_2 |\mathcal{X}|. \tag{19}$$

This upper bound can be approached at sufficiently high SNRs where the codewords are reliably distinguishable. We note that (19) implies that the number of bits which can be conveyed in each pulse cannot be larger than the number of bits needed for representing the different codewords. The upper bound in (19) may be approximated using Stirling's formula via (12).

The achievable rate analysis provides a measure for quantifying the communication capabilities of MAJoRCom. In the numerical study in Section V we demonstrate that in low SNRs, MAJoRCom is capable of achieving higher rates than using individual dedicated communication waveforms, without interfering or even affecting the radar performance. Nonetheless, this information-theoretic framework does not account for practical considerations such as computational burden at the receiver, motivating the reduced complexity implementation presented in the following section.

IV. Reduced Decoding Complexity Implementation

As discussed in the introduction, one of the major benefits of MAJoRCom stems from its usage of narrowband signals and relatively low computational complexity, which imply that it can be implemented using simple hardware components. However, while generating and transmitting the communication signal by MAJoRCom does not require heavy computations, decoding the transmitted index-modulated message by the communication receiver may entail a substantial computational burden. Consequently, in this section we propose methods for reducing the decoding complexity.

We begin by discussing the optimal maximum likelihood (ML) symbol decoding scheme in Subsection IV-A. Then, we present two approaches for mitigating its complexity: In Subsection IV-B we propose a sub-optimal decoding method, which affects only the communication receiver. Then, we propose a modified codebook design which facilitates decoding by reducing the number of codewords used by MAJoRCom in Subsection IV-C. The change of codebook may affect the radar beam pattern, however the simulation results present later in Section V demonstrate that this change has minimum influence on range, Doppler and angle estimates of radar targets. Those two approaches are independent of each other, and can be used either simultaneously or individually, depending on the computational abilities of the communications receiver.

A. Optimal ML Decoder

To detect the conveyed symbols, the receiver estimates both the selected frequencies and allocated antenna indices. Since the entries of the noise matrix $\boldsymbol{N}_{\mathrm{C}}$ are i.i.d. Gaussian and the codewords are equiprobable, the detector which minimizes the probability of error is the ML estimator of the frequency indices $\{c_k\}$ and the antenna allocations $\{\boldsymbol{P}_k\}$ [49, Ch. 5.1]. From (14), the ML estimator is given by

$$\left\{\hat{c}_k, \widehat{\boldsymbol{P}}_k\right\}_{k=0}^{K-1} = \underset{\{c_k, \boldsymbol{P}_k\}}{\arg\min} \left\| \boldsymbol{Y}_{\mathrm{C}} - \sum_{k=0}^{K-1} \boldsymbol{H}\boldsymbol{P}_k \boldsymbol{w}_k \boldsymbol{\psi}_{c_k}^T \right\|_F^2, \tag{20}$$

where $\|\cdot\|_F$ denotes the Frobenius norm. Here, the pointing direction θ in $\boldsymbol{w}_k$ is assumed known. Since the frequency indices $\{c_k\}$ and the selection matrices $\{\boldsymbol{P}_k\}$ are integers and binary matrices, respectively, the above problem is generally NP-hard. In particular, solving (20) involves exhaustively searching over $\mho$ and $\mathcal{P}$, resulting in high computational complexity. This increased complexity settles with the fact that optimal index modulation decoding is typically computationally complex [35].

Various low complexity methods have been proposed for different forms of index modulation, see, e.g., [35, Tbl. 1]. However, as our form of index modulation, in which all the transmitted information is embedded in the selection of the frequencies and their allocation among antennas (without additional digital modulation signals), is unique, in the next subsection we design a dedicated low-complexity decoder.

B. Low Complexity Receiver Design

Here, we present a sub-optimal detection method. Instead of jointly estimating $\{c_k, \boldsymbol{P}_k\}$ in (20), our proposed strategy operates in an iterative manner: It first initializes the frequency estimates $\{c_k\}$ using sparse recovery, possibly via simple fast Fourier transformation (FFT) followed by thresholding. Then, we iteratively recover the spatial selection matrices $\{\boldsymbol{P}_k\}$, and refine the estimation of $\{c_k\}$ in an alternating fashion.

1) Frequency Initialization: In the first step, we obtain an initial estimation of the transmitted frequencies. To that aim, we rewrite the model (14) as

$$\boldsymbol{Y}_{\mathrm{C}}^T = \boldsymbol{\Psi}\boldsymbol{A} + \boldsymbol{N}_{\mathrm{C}}^T, \tag{21}$$

where $\boldsymbol{\Psi} = [\boldsymbol{\psi}_0, \boldsymbol{\psi}_1, \ldots, \boldsymbol{\psi}_{M-1}] \in \mathbb{C}^{L_T \times M}$ contains all M sub-bands, and thus is a-priori known. The matrix $\boldsymbol{A} \in \mathbb{C}^{M \times L_{\mathrm{C}}}$ depends on the frequency indices $\{c_k\}$: When there exists an index $c_k = m$, the transpose of the m-th row of $\boldsymbol{A}$ is given by

$$\left[\boldsymbol{A}^T\right]_m = \boldsymbol{H}\boldsymbol{P}_k\boldsymbol{w}_k \in \mathbb{C}^{L_{\mathrm{C}}}, \tag{22}$$

while otherwise $[\boldsymbol{A}^T]_m = \boldsymbol{0}_{L_{\mathrm{C}}}$. We regard $\boldsymbol{A}$ as an unknown variable, which has to be estimated. After $\boldsymbol{A}$ is estimated as $\widehat{\boldsymbol{A}}$, the frequency indices $\{c_k\}$ are recovered from the non-zero rows (or the K rows with largest norms) of $\widehat{\boldsymbol{A}}$.

The matrix $\widehat{\boldsymbol{A}}$ is obtained by solving (21), which can be accomplished using a sparse recovery method [50]. The sparsity of $\boldsymbol{A}$ arises naturally, which means the number of nonzero rows in $\boldsymbol{A}$ (also referred to as the sparsity level) is far less than the number of observations L_T. This sparse property stems from the facts that CAESAR uses only a small portion of frequencies, i.e., $K \ll M$, to guarantee frequency agility and that the number of samples is generally no less than the number of frequencies, i.e., $L_T \geq M$, as long as the pulse duration is no less than $1/\Delta f$, implying $K \ll L_T$. Furthermore, we assume that the sparsity level K is known, which can be used as a threshold in many sparse recovery algorithms. For example, in greedy approaches like OMP [50], the number of iterations is determined by K, while in ℓ_1 minimization based methods like Lasso [50], the K rows with largest norm are identified from the estimated result $\widehat{\boldsymbol{A}}$. The selected K rows indicate the frequency indices $\{c_k\}$.

The sparse recovery procedure can be simplified when the pulse duration is an integer multiple of $1/\Delta f$, i.e., $T_p = n/\Delta f$, $n \in \mathbb{Z}^+$. To see this, note that the number of samples equals $L_T = nM + 1$, under the assumption that both the rising and falling edges of the pulse are ideally sampled by the receiver. While in a practical scenario operating in the presence of asynchronization, the effective pulse duration is generally slightly

shorter than the ideal value, leading to $L_T = nM$. Here, we let $L_T = nM$ in which case $\boldsymbol{\Psi}$ in (21) consists of M columns from the $L_T \times L_T$ FFT matrix. In such settings, in which the columns of $\boldsymbol{\Psi}$ are orthogonal (or approximately orthogonal), simple projection and thresholding may achieve comparable support recovery performance as more computationally complex iterative sparse recovery methods. In particular, when the columns of $\boldsymbol{\Psi}$ are orthogonal, projection and thresholding recovers $\widehat{\boldsymbol{A}}$ via

$$\widehat{\boldsymbol{A}} = \boldsymbol{\Psi}^H \boldsymbol{Y}_{\mathrm{C}}^T, \tag{23}$$

which can be computed using FFT. We then sort the norms of the rows, $\|[\boldsymbol{A}^T]_m\|_2$, in a descending order, and identify the first K rows, which correspond to the frequency indices $\{c_k\}$. The use of FFT is most suitable when $T_p \approx n/\Delta f$, and its main benefit is its low computational complexity. When this approximation does not hold, one can utilize any sparse recovery method for obtaining $\widehat{\boldsymbol{A}}$. In the extreme case where $K = M = L_T$, i.e., $\boldsymbol{A}$ does not follow a sparse structure, one may estimate $\boldsymbol{A}$ using matched filtering, as in (23).

2) Spatial Decoder: After the frequency indices are recovered as $\{\hat{c}_k\}$, the ML estimator (20) becomes

$$\left\{\widehat{\boldsymbol{P}}_k\right\}_{k=0}^{K-1} = \underset{\{\boldsymbol{P}_k\}}{\arg\min} \left\| \boldsymbol{Y}_{\mathrm{C}} - \sum_{k=0}^{K-1} \boldsymbol{H}\boldsymbol{P}_k \boldsymbol{w}_k \boldsymbol{\psi}_{\hat{c}_k}^T \right\|_F^2, \tag{24}$$

which jointly optimizes K selection matrices $\{\boldsymbol{P}_k\}_{k=0}^{K-1}$ and can be solved by exhaustive search over $\mathcal{P}$. Here, $\{\boldsymbol{w}_k\}$ are calculated with the obtained $\{\hat{c}_k\}$. As directly solving (24) may still be difficult, we next introduce a greedy approach that solves each selection matrix $\boldsymbol{P}_k$ sequentially to reduce the computational burden.

Denote by $\hat{c}_0, \hat{c}_1, \ldots, \hat{c}_{K-1}$ the obtained frequency indices $\{c_k\}$ in such an order that the corresponding rows of $\widehat{\boldsymbol{A}}$ satisfy $\|[\widehat{\boldsymbol{A}}^T]_{\hat{c}_0}\|_2 \geq \|[\widehat{\boldsymbol{A}}^T]_{\hat{c}_1}\|_2 \geq \cdots \geq \|[\widehat{\boldsymbol{A}}^T]_{\hat{c}_{K-1}}\|_2$. According to (22), we write the $\hat{c}_k$-th row of $\widehat{\boldsymbol{A}}$ as

$$\left[\widehat{\boldsymbol{A}}^T\right]_{\hat{c}_k} = \widetilde{\boldsymbol{H}}\boldsymbol{p}_k + \boldsymbol{n}_k, \quad k = 0, 1, \ldots, K-1, \tag{25}$$

where $\widetilde{\boldsymbol{H}} := \boldsymbol{H}\mathrm{diag}(\boldsymbol{w}_k)$; $\mathrm{diag}(\boldsymbol{w}_k)$ denotes the diagonal matrix with entries defined in $\boldsymbol{w}_k$; $\boldsymbol{p}_k \in \{0,1\}^{L_{\mathrm{R}}}$ contains the diagonal entries in $\boldsymbol{P}_k$; and $\boldsymbol{n}_k$ denotes the estimate errors in $[\widehat{\boldsymbol{A}}^T]_{c_k}$. Recall that in each pulse, every antenna is assigned to a single frequency, and thus $\sum_{i=0}^{K-1} \boldsymbol{p}_i = \boldsymbol{1}_{L_{\mathrm{R}}}$, implying that $\boldsymbol{p}_k \wedge (\sum_{i=0}^{k-1} \boldsymbol{p}_i) = \boldsymbol{0}_{L_{\mathrm{R}}}$, where $\wedge$ denotes the entry-wise logical and operation. The fact that the unknown vectors $\{\boldsymbol{p}_k\}$ take binary values and are subject to this joint constraint gives rise to the following sequential approach. Here, we assume that $\boldsymbol{p}_0, \boldsymbol{p}_1, \ldots, \boldsymbol{p}_{k-1}$ have been recovered prior to $\boldsymbol{p}_k$. Then, we use (25) to formulate the recovery of $\boldsymbol{p}_k$ as:

$$\begin{aligned} \hat{\boldsymbol{p}}_k = & \underset{\boldsymbol{p}_k}{\arg\min} \left\| \left[\widehat{\boldsymbol{A}}^T\right]_{c_k} - \widetilde{\boldsymbol{H}}\boldsymbol{p}_k \right\|_2^2, \\ & \text{s.t.} \quad \boldsymbol{p}_k \wedge \left(\sum_{i=0}^{k-1} \boldsymbol{p}_i\right) = \boldsymbol{0}_{L_{\mathrm{R}}}, \ \|\boldsymbol{p}_k\|_1 = L_K. \end{aligned} \tag{26}$$

Problem (26) is solved using exhaustive search since $\boldsymbol{p}_k$ takes binary values. There are $\binom{L_{\mathrm{R}} - kL_K}{L_K}$ possible values for each $\boldsymbol{p}_k$, and at most a total of $K\binom{L_{\mathrm{R}}}{L_K}$ evaluations need to be carried out to recover all vectors $\{\boldsymbol{p}_k\}$. Compared with the optimal ML method (24), which requires approximately $|\mathcal{P}| \approx \binom{L_{\mathrm{R}}}{L_K}^K$ searches once the frequency indices $\{c_k\}$ are recovered, the sub-optimal method reduces the complexity significantly. In our numerical analysis in Section V we show that the proposed low-complexity decoder is capable of achieving BER performance which is comparable to the computationally complex ML decoder.

Algorithm 1: Non-Iterative Low Complexity Decoder.

Input: $\boldsymbol{Y}_C$, $\boldsymbol{\Psi}$, K.

Steps:

(1) Compute $\widehat{\boldsymbol{A}}$ via sparse recovery, possibly using (23) if $T_p \approx n/\Delta f$, and calculate the norms of the rows of $\widehat{\boldsymbol{A}}$.

(2) Sort these norms in a descending order, recovering $\{\hat{c}_k\}$.

(3) Apply ML-based spatial decoder via (24), or perform greedy spatial decoding, i.e., sequentially solve (26).

Output: $\{\hat{c}_k, \widehat{\boldsymbol{P}}_k\}_{k=0}^{K-1}$.

The proposed method obtains a coarse estimate of $\{c_k, \boldsymbol{P}_k\}$, and is summarized in Algorithm 1. This coarse estimate can be later refined by updating $\{c_k\}$ and $\{\boldsymbol{P}_k\}$, as well as $\widehat{\boldsymbol{A}}$ which is used in estimating both $\{c_k\}$ and $\{\boldsymbol{P}_k\}$, in an alternating manner. The method to update $\{\boldsymbol{P}_k\}$ using an estimate of $\{c_k\}$ and $\widehat{\boldsymbol{A}}$ is based on the above, while the refining of $\{c_k\}$ and $\widehat{\boldsymbol{A}}$ based on an estimate of $\{\boldsymbol{P}_k\}$ is detailed in the subsequent frequency refinement step.

3) Frequency Refinement: With the estimates $\{\widehat{\boldsymbol{P}}_k\}_{k=0}^{K-1}$, we refine the frequency codes $\{c_k\}_{k=0}^{K-1}$. According to (20), the optimization problem becomes

$$\{\hat{c}_k\}_{k=0}^{K-1} = \underset{\{c_k\}}{\arg\min} \left\| \boldsymbol{Y}_{\mathrm{C}} - \sum_{k=0}^{K-1} \widetilde{\boldsymbol{H}}_k \boldsymbol{w}_k \boldsymbol{\psi}_{c_k}^T \right\|_F^2, \tag{27}$$

where $\widetilde{\boldsymbol{H}}_k := \boldsymbol{H}\widehat{\boldsymbol{P}}_k \in \mathbb{C}^{L_{\mathrm{C}} \times L_{\mathrm{R}}}$ and $\boldsymbol{w}_k$ is determined by c_k. Since the set $\{c_k\}$ consists of K distinct indices in the range $\{0, 1, \ldots, M-1\}$, (27) should be solved via exhaustive search, requiring a total of $\binom{M}{K}$ evaluations. Similarly to the aforementioned spatial decoder that utilizes a greedy approach, one may also estimate the frequency codes sequentially to reduce the computation, as detailed next.

In particular, when recovering c_k, let $\{\hat{c}_m\}_{m=0}^{k-1}$ be the previously obtained frequency indices. The estimation of c_k can be formulated by rewriting (27) as

$$\begin{aligned} \hat{c}_k = & \underset{c_k}{\arg\min} \left\| \boldsymbol{Y}_{\mathrm{C}} - \sum_{m=0}^{k-1} \widetilde{\boldsymbol{H}}_m \boldsymbol{w}_m \boldsymbol{\psi}_{\hat{c}_m}^T - \widetilde{\boldsymbol{H}}_k \boldsymbol{w}_k \boldsymbol{\psi}_{c_k}^T \right\|_F^2, \\ & \text{s.t.} \quad c_k \in \{0, 1, \ldots, M-1\} \backslash \{\hat{c}_m\}_{m=0}^{k-1}. \end{aligned} \tag{28}$$

In this greedy approach, only a total of $\sum_{k=0}^{K-1}(M-k) = KM - \frac{K(K-1)}{2}$ evaluations are required, which is much less than its exhaustive search counterpart.

Next, we use the estimates of $\{\hat{c}_k, \widehat{\boldsymbol{P}}_k\}$ to obtain a refined estimate of $\widehat{\boldsymbol{A}}$, which is used in the greedy spacial decoder (26). In the initial steps (as indicated in Algorithm 1), in which an

Algorithm 2: Iterative Low Complexity Decoder.

Input: $\boldsymbol{Y}_C$, $\boldsymbol{\Psi}$, K, maximal iteration $i_{\max}$.
Initialization:
(1) $i \leftarrow 1$.
(2) Obtain $\{\hat{c}_k^{(0)}, \widehat{\boldsymbol{P}}_k^{(0)}\}_{k=0}^{K-1}$ and $\widehat{\boldsymbol{A}}^{(0)}$ using Algorithm 1.
While $i < i_{\max}$:
(3) Obtain $\{c_k^{(i)}\}_{k=0}^{K-1}$ via ML-based frequency refinement (27), or by sequentially solving (28).
(4) Evaluate $\widehat{\boldsymbol{A}}^{(i)}$ using (29).
(5) Compute $\{\widehat{\boldsymbol{P}}_k^{(i)}\}_{k=0}^{K-1}$ by applying ML-based spatial decoding (24), or by sequentially solving (26).
(6) $i \leftarrow i+1$.
Output: $\{\hat{c}_k^{(i_{\max}-1)}, \widehat{\boldsymbol{P}}_k^{(i_{\max}-1)}\}_{k=0}^{K-1}$.

estimate of $\{\hat{c}_k, \widehat{\boldsymbol{P}}_k\}$ is not available, $\widehat{\boldsymbol{A}}$ is computed with sparse recovery. Having obtained $\{\hat{c}_k, \widehat{\boldsymbol{P}}_k\}$, we refine the value of $\widehat{\boldsymbol{A}}$. In particular, by (22), $\widehat{\boldsymbol{A}}$ is computed by setting its $\hat{c}_k$-th row to

$$\left[\widehat{\boldsymbol{A}}^T\right]_{\hat{c}_k} = \boldsymbol{H}\widehat{\boldsymbol{P}}_k\boldsymbol{w}_k, \tag{29}$$

while fixing the remaining rows to be the all-zero vector. The resulting algorithm, which uses the spatial decoder and frequency refinement steps in Subsection IV-B2 and IV-B3 to update $\{\boldsymbol{P}_k\}_{k=0}^{K-1}$ and $\{c_k\}_{k=0}^{K-1}$, respectively, is summarized in Algorithm 2.

4) Complexity Analysis: Algorithms 1-2 are proposed in order to tackle the increased computational burden associated with index modulation communications [35], which MAJoRCom exploits to integrate digital messages into agile radar waveforms. These methods allow the communication receiver to balance decoding accuracy and complexity, where the latter is dictated by the selection of which decoding method to use, e.g., ML-based decoders or sequential methods, as well as the setting of the system parameters. To understand how each setting affects the overall complexity, in the following we analyze the computational burden of Algorithm 2, quantified in terms of number of complex multiplications. Note that Algorithm 2 specializes to Algorithm 1 by setting the number of iterations to $i_{\max} = 1$.

The complexity of Algorithm 2 is dominated by the iterative refinement in Step (3), which is carried out $i_{\max}-1$ times, and the spatial estimation in Step (5), which is carried out $i_{\max}$ times (being identical to Step (3) of Algorithm 1). The complexity of each of these steps depends on the decoding method used. For example, Step (3) is dominated by $M^2\binom{M}{K}L_C$ complex multiplications, when using the ML-based frequency refinement in (27), and by KM^2L_C complex multiplications, when relying on the sequential refinement in (28). Similarly, the spatial estimation in Step (5) involves either $\binom{L_R}{L_K}^K ML_C$ or $K\binom{L_R}{L_K}ML_C$ complex multiplications, when using the ML-based decoder (24) or the sequential method (26), respectively. Consequently, the computational complexity of Algorithm 2 is dominated by a term which is at most $i_{\max}\binom{L_R}{L_K}^K ML_C + (i_{\max}-1)M^2\binom{M}{K}L_C$, when using ML-based methods for spatial decoding and spectral refinement. Alternatively, when using the sequential decoding methods, the overall complexity is dominated by the term $i_{\max}\binom{L_R}{L_K}KML_C + (i_{\max}-1)(KM - \frac{K(K-1)}{2})ML_C$.

The above analysis indicates that the complexity of the ML-based decoders grows rapidly with K. Since these decoders are capable of achieving improved decoding accuracy compared to the sequential methods, as also numerically demonstrated in Section V, our analysis further reveals the inherent accuracy - complexity tradeoff arising when using index modulation communication schemes. Our proposed decoding algorithms provide means for balancing these important measures by selecting the decoding method and the algorithm parameters, e.g., the number of iterations $i_{\max}$.

C. Codebook Design

In the description of MAJoRCom in Section II, all possible options in $\mho$ and $\mathcal{P}$ are coded uniquely and used to carry different symbols. Fully exploiting the variety of these sets allows the achievable rate to approach the upper bound in (19) at sufficiently high SNR, as the different codewords can be reliably distinguished from one another. However, the computational complexity required to properly decode the message grows rapidly with the cardinality of these sets. Particularly, while detecting the used frequencies from $\mho$ can be implemented in a low complexity manner at the cost of some performance reduction, recovering the antenna allocation from $\mathcal{P}$ typically requires an exhaustive search, as discussed in the previous subsection. Therefore, in order to facilitate accurate decoding under computational complexity constraints, we now propose a codebook design which makes full use of $\mho$ while utilizing a subset of N_b codewords from $\mathcal{P}$, thus balancing achievable rate and computational burden at the receiver.

Our goal is to design a constellation set, which is a subset of $\mathcal{P}$, such that the ability of the receiver to distinguish between different codewords is improved. To that aim, we first discuss the design criterion, which yields a high dimensional NP-hard max-min problem. To solve it, we first apply a dimension reduction approach, after which we propose a sub-optimal solution.

1) Design Criterion: When the impact on the radar function is not accounted for, the proper codebook design objective is to maximize the minimum distance between any two codewords, $\{\boldsymbol{P}_k^{(i)}\}_{k=0}^{K-1}$ and $\{\boldsymbol{P}_k^{(j)}\}_{k=0}^{K-1}$, or equivalently, $\{\boldsymbol{p}_k^{(i)}\}_{k=0}^{K-1}$ and $\{\boldsymbol{p}_k^{(j)}\}_{k=0}^{K-1}$. In particular, it follows from (24) that the distance,

$$\left\| \sum_{l=0}^{K-1} \boldsymbol{H}\boldsymbol{P}_l^{(i)}\boldsymbol{w}_l\boldsymbol{\psi}_{c_l^{(i)}}^T - \sum_{k=0}^{K-1} \boldsymbol{H}\boldsymbol{P}_k^{(j)}\boldsymbol{w}_k\boldsymbol{\psi}_{c_k^{(j)}}^T \right\|_F^2, \tag{30}$$

dominates the error probability between the i-th and j-th symbols. Since we optimize the minimum distance with respect to the antenna allocations $\{\boldsymbol{p}_k\}$, we henceforth focus on the setting where the set of frequency indices are the same in those symbols, i.e., $\{c_k^{(i)}\}_{k=0}^{K-1}$ equals $\{c_k^{(j)}\}_{k=0}^{K-1}$. This setting generally leads to a smaller distance in comparison with the unequal case, and can thus be considered as a worst case scenario.

When the frequency modulations are orthogonal, i.e., $\boldsymbol{\psi}_{m_1}^H\boldsymbol{\psi}_{m_2} = 0,\ m_1 \neq m_2,\ m_1, m_2 \in \mathcal{M}$, which holds when T_p is an integer multiple of $1/\Delta f$, the distance between two codewords may be simplified to

$$\text{H-Dist}_{i,j} := \sum_{k=0}^{K-1} \left\| \widetilde{\boldsymbol{H}}\boldsymbol{p}_k^{(i)} - \widetilde{\boldsymbol{H}}\boldsymbol{p}_k^{(j)} \right\|_2^2. \tag{31}$$

The distance (31) is upper bounded by the largest eigenvalue of $\widetilde{\boldsymbol{H}}$ times $\text{Dist}_{i,j}$, which is defined as

$$\text{Dist}_{i,j} := \sum_{k=0}^{K-1} \left\| \boldsymbol{p}_k^{(i)} - \boldsymbol{p}_k^{(j)} \right\|_2^2. \tag{32}$$

We propose a codebook design to find a subset $\mathcal{P}^{\#} \subset \mathcal{P}$ of cardinality N_b that maximizes the distance

$$\max_{\mathcal{P}^{\#} \subset \mathcal{P}} \min_{i,j \in \mathcal{P}^{\#}, i \neq j} \text{Dist}_{i,j}, \quad \text{s.t. } \left|\mathcal{P}^{\#}\right| = N_b. \tag{33}$$

We note that (33) is still NP-hard to solve. Although the objective in (33) can be considered as the minimal Hamming distance, standard codebook desgins based on this criterion, see [49, Ch. 8], cannot be used here. The reason is that our codewords are subject to the additional unique constraint $\sum_{k=0}^{K-1} \boldsymbol{p}_k^{(i)} = \boldsymbol{1}_{L_{\text{R}}}$, which does not appear in standard binary codebooks. Thus, we propose a codebook design based on projection into a lower dimensional plane, described next.

2) Dimension Reduction of the Constellation: Here, we use a binary-valued vector $\boldsymbol{p}^{(i)} := [(\boldsymbol{p}_0^{(i)})^T, (\boldsymbol{p}_1^{(i)})^T, \ldots, (\boldsymbol{p}_{K-1}^{(i)})^T]^T \in \{0,1\}^{KL_{\text{R}}}$ to represent the i-th codeword $\{\boldsymbol{p}_k^{(i)}\}$. We then propose to project the original codeword into a real-valued L_{D}-dimensional plane, i.e., $\boldsymbol{p}^{(i)} \mapsto \widetilde{\boldsymbol{p}}^{(i)} \in \mathbb{R}^{L_{\text{D}}}$, such that the distances between codewords are maintained

$$\widetilde{d}\langle i,j \rangle := \|\widetilde{\boldsymbol{p}}^{(i)} - \widetilde{\boldsymbol{p}}^{(j)}\|_2^2 = \text{Dist}_{i,j}, \tag{34}$$

where $i,j = 0,1,\ldots,|\mathcal{P}|-1$. It is easy to verify that (34) holds when there exist an orthogonal matrix $\boldsymbol{U} \in \mathbb{R}^{KL_{\text{R}} \times KL_{\text{R}}}$ and a constant vector $\boldsymbol{a} \in \mathbb{R}^{KL_{\text{R}}}$ such that

$$\boldsymbol{p}^{(i)} = \boldsymbol{U} \begin{bmatrix} \widetilde{\boldsymbol{p}}^{(i)} \\ \boldsymbol{0}_{KL_{\text{R}}-L_{\text{D}}} \end{bmatrix} + \boldsymbol{a}. \tag{35}$$

To find such $\boldsymbol{U}$, $\boldsymbol{a}$ and $\widetilde{\boldsymbol{p}}^{(i)}$, we use principal component analysis (PCA) [51]. Denote the codebook matrix by $\boldsymbol{D} := [\boldsymbol{p}^{(0)}, \boldsymbol{p}^{(1)}, \ldots, \boldsymbol{p}^{(|\mathcal{P}|-1)}] \in \{0,1\}^{KL_{\text{R}} \times |\mathcal{P}|}$, and the dimension reduced matrix by $\widetilde{\boldsymbol{D}} := [\widetilde{\boldsymbol{p}}^{(0)}, \widetilde{\boldsymbol{p}}^{(1)}, \ldots, \widetilde{\boldsymbol{p}}^{(|\mathcal{P}|-1)}] \in \mathbb{R}^{L_{\text{D}} \times |\mathcal{P}|}$, respectively. Then, (35) becomes

$$\boldsymbol{D} = \boldsymbol{U} \begin{bmatrix} \widetilde{\boldsymbol{D}} \\ \boldsymbol{0}_{(KL_{\text{R}}-L_{\text{D}}) \times |\mathcal{P}|} \end{bmatrix} + \boldsymbol{a} \cdot \boldsymbol{1}_{|\mathcal{P}|}^T. \tag{36}$$

Noticing that $\boldsymbol{p}^{(i)}$ has identical average, i.e., $\frac{1}{KL_{\text{R}}} \boldsymbol{1}_{KL_{\text{R}}}^T \boldsymbol{p}^{(i)} = \frac{1}{K}$, we first normalize the columns of $\boldsymbol{D}$ to zero mean by

$$\overline{\boldsymbol{D}} = \boldsymbol{D} - \frac{1}{K} \boldsymbol{1}_{KL_{\text{R}} \times |\mathcal{P}|}. \tag{37}$$

We next perform an SVD decomposition on $\overline{\boldsymbol{D}}$, i.e.,

$$\overline{\boldsymbol{D}} = \boldsymbol{U} \boldsymbol{\Sigma} \boldsymbol{V}^T, \tag{38}$$

where $\boldsymbol{U} \in \mathbb{R}^{KL_{\text{R}} \times KL_{\text{R}}}$ and $\boldsymbol{V} \in \mathbb{R}^{|\mathcal{P}| \times |\mathcal{P}|}$ are unitary matrices, $\boldsymbol{U}\boldsymbol{U}^T = \boldsymbol{U}^T\boldsymbol{U} = \boldsymbol{I}_{KL_{\text{R}}}$, $\boldsymbol{V}\boldsymbol{V}^T = \boldsymbol{V}^T\boldsymbol{V} = \boldsymbol{I}_{|\mathcal{P}|}$, and $\boldsymbol{\Sigma} \in \mathbb{R}^{KL_{\text{R}} \times |\mathcal{P}|}$ is a diagonal matrix with $[\boldsymbol{\Sigma}]_{i,i}$, $i \leq KL_{\text{R}}$, being the singular values of $\overline{\boldsymbol{D}}$. We estimate L_{D}, which is often regarded as the intrinsic dimension of the original codewords, as the number of nonzero singular values, i.e., the rank of $\overline{\boldsymbol{D}}$, and the transpose of the new codewords are given by

$$\widetilde{\boldsymbol{D}}^T = \boldsymbol{V} \left[\boldsymbol{\Sigma}^T\right]_{\{0,1,\ldots,L_{\text{D}}-1\}}. \tag{39}$$

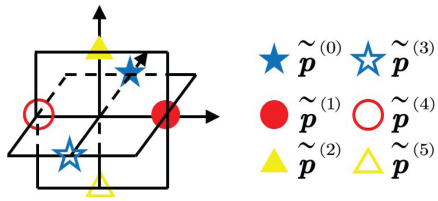

Fig. 4. A constellation of dimension reduced codewords, $L_{\text{R}} = 4$, $K = 2$, and $L_K = 2$.

With $\boldsymbol{a} = 1/K \boldsymbol{1}_{KL_{\text{R}}}$ it can be verified that (36) holds and codewords $\widetilde{\boldsymbol{D}}$ preserve the distances as in (34).

It is worth noting that the special structure of $\boldsymbol{p}^{(i)}$ results in some symmetry of the distances $\text{Dist}_{i,j}$. To see this, we define the distance matrix $\boldsymbol{R} \in \mathbb{Z}^{|\mathcal{P}| \times |\mathcal{P}|}$ with entries

$$[\boldsymbol{R}]_{i,j} = \text{Dist}_{i,j}, \quad i,j = 0,1,\ldots,|\mathcal{P}|-1. \tag{40}$$

The distance matrix has the following properties.

Proposition 2: The matrix $\boldsymbol{R}$ is symmetric and its diagonal entries are zeros, i.e,. $[\boldsymbol{R}]_{i,j} = [\boldsymbol{R}]_{j,i}$ and $[\boldsymbol{R}]_{i,i} = 0$, $i,j = 0,1,\ldots,|\mathcal{P}|-1$. Furthermore, each row of $\boldsymbol{R}$ is a permutation of the first row in $\boldsymbol{R}$.

Proof: A proof is given in the Appendix. ■

Proposition 2 implies that, given a set $\mathcal{P}$ of different possible antenna allocation codewords, the calculation of the distance matrix $\boldsymbol{R}$ is far less computationally complex than evaluating the distance between each possible pair of elements of $\mathcal{P}$ in a straightforward manner.

We take $L_{\text{R}} = 4$, $K = 2$ and $L_K = 2$ as an example to demonstrate the dimension reduction. When $L_{\text{D}} = 2$ or 3, we find that the projected codebook can be visualized conveniently using $\widetilde{\boldsymbol{p}}$. To see this, recall that there are 6 possible spatial selection patterns as explained by (9). The original codewords, $\{\boldsymbol{p}_0^{(i)}, \ldots, \boldsymbol{p}_{K-1}^{(i)}\}$, $i = 0,\ldots,5$, have $KL_{\text{R}} = 8$ dimensions, and are difficult to display. The entries of the distance matrix here are given by

$$[\boldsymbol{R}]_{i,j} = \begin{cases} 0 & i = j, \\ 8 & |i-j| = 3, \\ 4 & \text{otherwise.} \end{cases}$$

After dimensionality reduction, one obtains the following three-dimensional representation of the codewords: $\widetilde{\boldsymbol{p}}^{(0)} = [0, \sqrt{2}, 0]^T$, $\widetilde{\boldsymbol{p}}^{(1)} = [\sqrt{2}, 0, 0]^T$, $\widetilde{\boldsymbol{p}}^{(2)} = [0, 0, \sqrt{2}]^T$, and $\widetilde{\boldsymbol{p}}^{(3)} = -\widetilde{\boldsymbol{p}}^{(0)}$, $\widetilde{\boldsymbol{p}}^{(4)} = -\widetilde{\boldsymbol{p}}^{(1)}$, $\widetilde{\boldsymbol{p}}^{(5)} = -\widetilde{\boldsymbol{p}}^{(2)}$. We can verify that $\widetilde{d} < i,j >= [\boldsymbol{R}]_{i,j}$. The resulting three-dimennsional constellation set is depicted in Fig. 4.

3) Design of the Constellation Set: After dimension reduction, the codebook design problem (33) becomes

$$\max_{\mathcal{P}^{\#} \subset \mathcal{P}} \min_{i,j \in \mathcal{P}^{\#}, i \neq j} \widetilde{d} < i,j >, \text{ s.t. } \left|\mathcal{P}^{\#}\right| = N_b. \tag{41}$$

We propose the following sub-optimal approach to design a codebook based on (41): Using clustering methods such as k-means, the codewords $\widetilde{\boldsymbol{D}}$ can be divided into N_b classes. The codeword which is the nearest to the center point of the class is used to represent the class in the final codebook. Since clustering methods typically maximize the distances between classes, the proposed codebook is expected to have a large minimal distance, thus approaching the solution to (41).

Reducing the number of different antenna allocations affects the spatial agility and radiation pattern of the radar scheme, and thus potentially impacts the accuracy of range, Doppler or angular parameters of CAESAR. Nonetheless, in the simulations study presented in Section V it is numerically demonstrated that the radar performance degradation due to using the proposed reduced cardinality codebook is minimal.

V. Simulations

In this section we numerically evaluate the performance of MAJoRCom. Since the radar functionality of MAJoRCom is based on CAESAR and is not affected by the communication subsystem when the codewords are uniformly distributed over the complete codebook, we focus here on the communication functionality of MAJoRCom, and refer to [33] for a detailed study of its radar performance.

In particular, three aspects of the communication scheme are evaluated: First, in Subsection V-A the fundamental limits of the proposed system are compared to using different waveforms for communications and radar. Then, the proposed low complexity decoders are numerically compared to the optimal ML decoder in Subsection V-B. Next, in Subsection V-C the proposed reduced complexity codebook design approaches are evaluated along with their effect on radar performance. The effect of imbalanced codeword randomness on the radar performance of MAJoRCom is evaluated in Subsection V-D. Throughout this study, the initial frequency is $f_c = 1.9$ GHz, the frequency spacing is $\Delta f = 10$ MHz, and the number of frequencies utilized at each pulse is $K = 2$ unless specifically stated otherwise.

A. Achievable Rate

Our achievable rate analysis quantifies the communication capabilities of MAJoRCom, facilitating its comparison to other configurations. As a numerical example, we consider a scenario with 4 transmit and receive antennas, i.e., $L_{\mathrm{R}} = L_{\mathrm{C}} = 4$. The parameters of the proposed system are set to $\theta = \frac{\pi}{4}$, $d = 10\frac{c}{f_c}$, and the number of available frequencies is $M = 10$. The selection matrices used are given in (9). The overall number of codewords here is $|\mathcal{X}| = 270$, i.e., the maximal number of bits that can be conveyed in each pulse is $\log_2 |\mathcal{X}| \approx 8.1$. We consider two settings for the channel matrix $\boldsymbol{H}$: A spatial exponential decay channel, for which $[\boldsymbol{H}]_{l_1,l_2} = e^{-\frac{1}{4}(|l_1-l_2|+j(l_1-l_2)\pi)}$; and Rayleigh fading, where the entries of $\boldsymbol{H}$ are randomized from an i.i.d. zero-mean unit-variance proper-complex Gaussian distribution, and the achievable rate is averaged over 100 realizations.

For each channel, we evaluate the lower and upper bounds on the achievable rate computed via Proposition 1 and (19), respectively versus SNR, defined here as $1/\sigma^2$. This bound is compared to the rate achievable (in bits per channel use) when, instead of using the randomness of the radar scheme to convey bits, either the first antenna or the first two antennas are dedicated only for communications subject to a unit average power constraint, i.e., the same power as that of the radar pulse, neglecting the cross interference induced by radar and communications coexistence. This study allows to understand when the achievable rate of MAJoRCom, which originates from radar transmission, is comparable to using ideal dedicated communication transmitters, which are costly and induce mutual interference between radar and communications. The numerically evaluated achievable rates for the spatial decay channel and the Rayleigh fading channel are depicted in Figs. 5-6, respectively.

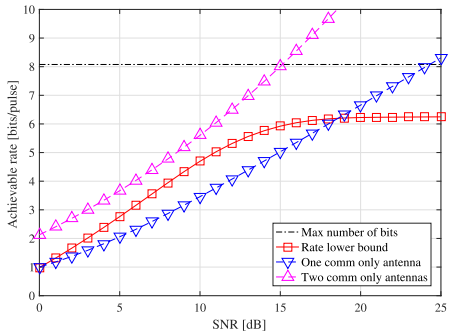

Fig. 5. Achievable rate comparison, spatial decay channel.

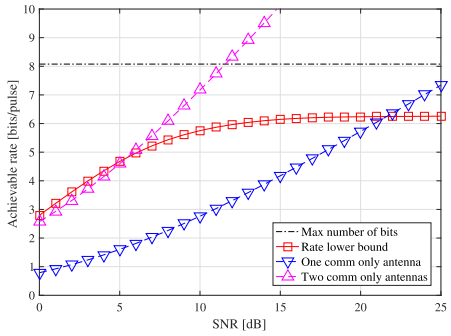

Fig. 6. Achievable rate comparison, Rayleigh fading channel.

Observing Figs. 5–6, we note that in relatively low SNRs, our proposed scheme achieves higher rates compared to using a dedicated communications antenna element *without impairing the radar performance*. For Rayleigh fading channels, it is demonstrated in Fig. 6 that MAJoRCom is capable of outperforming a system with two dedicated communication antennas for SNRs not larger than 5 dB. As the SNR increases, using dedicated communication antennas outperforms our proposed system as more and more bits can be reliably conveyed in a single channel symbol. However, it should be emphasized that by allocating some of the antenna elements for communications, the radar performance, which is considered as the primary user in our case, is degraded. Furthermore, in order to avoid coexistence issues, which we did not consider here, the communications and radar signals should be orthogonal, e.g., use distinct bands, thus reducing the radar bandwidth. Finally, the computation of the achievable rate with dedicated antennas assumes the transmitter has CSI and does not account for the need to utilize constant modulus waveforms; it is in fact achievable using Gaussian signaling [47, Ch. 9]. Consequently, the fact that, in addition to the practical benefits of our proposed scheme and its natural coexistence with the radar transmission, it is also capable of achieving communication rates comparable to using dedicated communication antennas, illustrates the gains of MAJoRCom.

B. Decoding Strategies

We now evaluate the BER performance of the reduced complexity decoders proposed in Subsection IV-B. To that aim, we first test the accuracy of the frequency initialization step in Algorithm 1. Next, we demonstrate the overall decoding performance, considering both the case in which the receiver

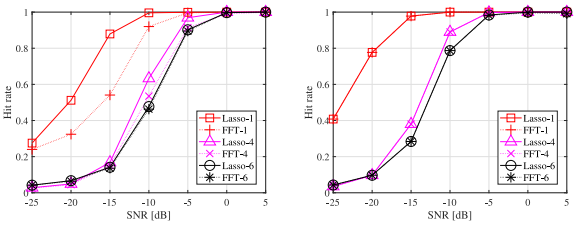

(a) $L_T = 8$ (b) $L_T = 16$

Fig. 7. Hit rates of frequency recovery with CS and FFT methods.

has accurate CSI, i.e., full knowledge of the channel matrix $\boldsymbol{H}$, as well as the performance when the receiver has only a noisy estimate of $\boldsymbol{H}$.

1) Frequency Initialization: We begin by evaluating the accuracy of the frequency initialization step. We use the compressed sensing (CS)-based block Lasso and FFT methods to recover the transmitted frequencies, and compare their performance under different sparsity levels and numbers of samples for each pulse. Block Lasso solves the following problem

$$\min_{\boldsymbol{A}} \|\boldsymbol{A}\|_{2,1} + \lambda \|\boldsymbol{Y}_{\mathrm{C}}^{T} - \boldsymbol{\Psi}\boldsymbol{A}\|_{F}, \tag{42}$$

where $\|\boldsymbol{A}\|_{2,1} = \sum_{i=0}^{M-1} \|[\boldsymbol{A}^T]_i\|_2$, $\|\cdot\|_F$ denotes Frobenius norm, and we set the regularization parameter to $\lambda = 0.5$. We fix the number of transmit and receive antennas to $L_{\mathrm{R}} = 12$ and $L_{\mathrm{C}} = 4$, respectively, and the channel matrix $\boldsymbol{H}$ is randomized as a zero-mean proper complex Gaussian matrix with i.i.d unit variance entries. The number of available frequencies is $M = 8$, and the beam is directed towards $\theta = 0$. The sampling rate used is $\frac{1}{T_s} = M\Delta f$. The number of channel outputs corresponding to each pulse is $L_T = T_p \cdot M\Delta f$. We let the number of selected frequencies in each pulse take the values $K = 1, 4, 6$, representing sparse, moderately sparse and non-sparse cases, respectively. The duration of the pulse is $T_p = 0.1$ and 0.2 μs, yielding $L_T = M = 8$ and $L_T = 2\tilde{}M = 16$ samples, respectively. Note that under these settings, the columns of $\boldsymbol{\Psi}$ are orthogonal.

The frequency recovery performance versus the SNR $1/\sigma^2$, is depicted in Fig. 7. Hit rates are utilized to evaluate the performance. A hit is proclaimed if a transmitted frequency is correctly identified. The results are obtained with 1000 trails and denoted by Lasso/FFT-K, where K represents the number of selected frequencies. We observe in both Figs. 7 a and 7 b that the hit rates decrease as the sparsity level increases. Comparing these two figures, we find that hit rates in Fig. 7 b are higher than the counterparts in Fig. 7 a, because more samples are available in the latter figure. According to the results in Fig. 7 a, in the cases that K is small, block Lasso outperforms FFT, while in the cases where K is close to M, the performance using an FFT for the initial frequency guess via (23) approaches that of the more complex block Lasso method. In Fig. 7 b, where more samples are available than that in Fig. 7 a, we find the performance of CS and FFT are nearly identical. Based on this observation that the accuracy of FFT-based frequency initialization approaches that of the block Lasso when L_T is reasonably large, we use FFT for the frequency initialization in the following simulations.

2) BER Performance: Next, we compare the BER performance of the proposed decoders, including the optimal ML decoder (20), denoted 'ML Decoder,' and the low complexity

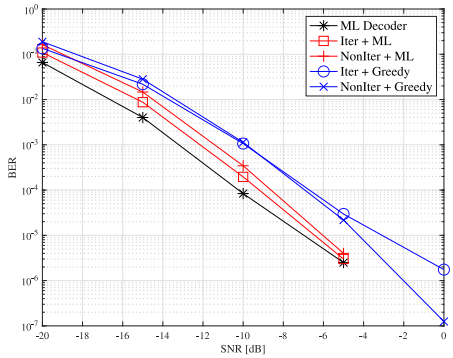

Fig. 8. Bit error rates of the proposed decoders.

decoders proposed in Subsection IV-B with non-iterative (Algorithm 1) and iterative settings (Algorithm 2). In Algorithm 1, we apply both an ML spatial decoder (24) as well as the sub-optimal sequential method with exhaustive search for (26) to recover the antenna selection vectors $\boldsymbol{p}_k$, denoted by 'NonIter + ML' and 'NonIter + Greedy,' respectively. In Algorithm 2, we test two approaches: One uses ML for both spatial and spectrum decoders, i.e. (24) and (27), denoted by 'Iter + ML'; the other one, denoted by 'Iter + Greedy,' uses greedy methods, i.e., (26) and (28) to recover the antenna selection vectors $\boldsymbol{p}_k$ and frequencies, respectively. In both iterative algorithms, i.e., 'Iter + ML' and 'Iter + Greedy,'which alternatively solve $\{\boldsymbol{P}_k\}$ and $\{c_k\}$, the maximum numbers of iterations is $i_{\max} = 10$, because we observe that 2 or 3 times of iterations are usually enough for the algorithms to converge to a stationary pair of $\{\boldsymbol{P}_k\}$ and $\{c_k\}$. The initial estimate of the matrix $\widehat{\boldsymbol{A}}$ is computed via (23).

We repeat the setup considered in the previous numerical study, with the exception of the following parameters: $L_{\mathrm{R}} = 6$, $M = 7$, $K = 2$, and $T_p = 1$ μs. Under this setting, the number of bits conveyed by frequency and spatial selections are $\lfloor \log_2 |\mathcal{U}| \rfloor = 4$ and $\lfloor \log_2 |\mathcal{P}| \rfloor = 4$, respectively. The BER performance versus the SNR, averaged over 10^6 trials is depicted in Fig. 8. As expected, the computationally complex optimal ML decoder achieves the lowest BER values. Our proposed sub-optimal decoders achieve a performance which scales similarly as the ML decoder with respect to SNR. In particular, the iterative and non-iterative decoders both achieve BER of 10^{-4} at SNR around -9 dB when combined with ML estimation, while the global ML decoder achieves the same BER at -10 dB, namely, an SNR gap of 1 dB. The corresponding SNR gap of the greedy sequential decoders is 3 dB. In particular, when using the greedy methods, it is observed in Fig. 8 that estimation refinement using Algorithm 2 does not necessarily improve the accuracy over the initial estimation in Algorithm 1. These results indicate that the proposed low complexity decoders are capable of achieving performance comparable to the ML decoder while substantially reducing the computational burden at the communication receiver.

3) BER Performance With Noisy CSI: In the simulation study presented in Fig. 8 the decoders operate with accurate knowledge of the channel matrix $\boldsymbol{H}$, i.e., full CSI. In practice, $\boldsymbol{H}$ must be estimated and estimation errors are usually inevitable. Here, we evaluate the influence of estimation error on the performance of the MAJoRCom decoders. We model the errors as an additive white Gaussian process. Hence, the perturbed channel matrix used by the decoders is represented by $\widehat{\boldsymbol{H}} = \boldsymbol{H} + \Delta\boldsymbol{H}$, where

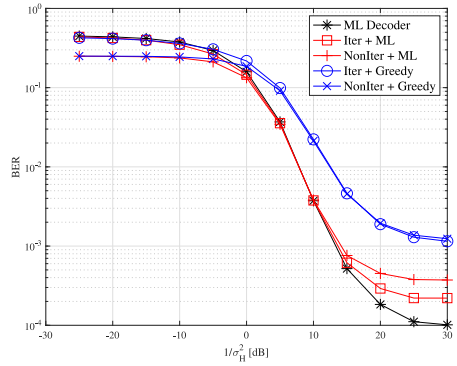

Fig. 9. BER values of the proposed decoders with noisy CSI.

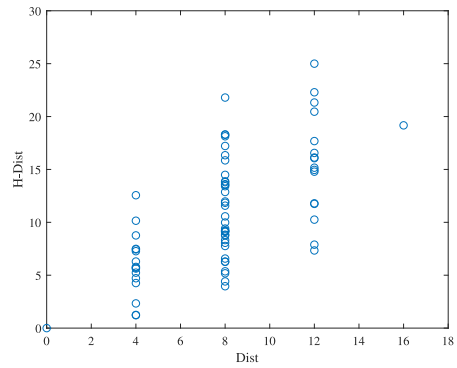

Fig. 10. H-Dist vs. Dist for $L_{\mathrm{C}} = 4$. Each circle represents a codeword.

$\boldsymbol{H}$ is the channel realization and $\Delta\boldsymbol{H}$ denotes the error matrix, which has i.i.d. entries of variance σ_H^2.

We depict the BER achieved by the decoders versus $1/\sigma_H^2$ in Fig. 9, where the SNR is set to -10 dB and the remaining configurations are the same as those used in Fig. 8. Comparing Fig. 9 and 8, we observe that noisy CSI affects severely affects the decoding performance for $1/\sigma_H^2$ lower than 20 dB. However, when the perturbations are of reasonably low level, e.g., $1/\sigma_H^2 > 25$ dB, the performance of the decoders approaches that achievable with full CSI.

C. Codebook Comparison

Here, we numerically study the codebook design proposed in Subsection IV-C, and evaluate the impact of the designed codewords on the decoding BER as well as the radar performance. The number of antennas is set to $L_{\mathrm{R}} = 8$, implying that the size of codebook is $|\mathcal{P}| = 70$ and the maximum number of bits is $\lfloor \log_2 |\mathcal{P}| \rfloor = 6$. Since the codebook does not affect the decoding procedure of the frequency indices, we assume that the transmitted frequencies are already recovered without errors. The remaining settings are the same as those used in the previous study.

We first evaluate the approximate design criterion minimizing (32), compared to the desired objective (31). The numerically computed distances (32) and (31), denoted 'Dist' and 'H-Dist,' respectively, are depicted in Fig. 10 for $L_{\mathrm{C}} = 4$, where we take a single realization of $\boldsymbol{H}$ as an example. Observing Fig. 10, we note an approximate monotonic relationship between two distances, which indicates that designing the codewords to minimize (32) also reduces the desired objective (31) proportionally. It is emphasized that when the number of receive antennas

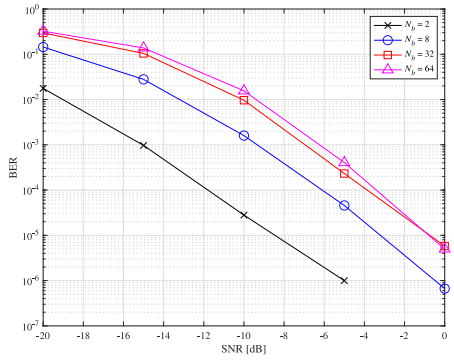

Fig. 11. BERs of the ML spatial decoder (24) for different codebook sizes.

L_{C} increases, the monotonicity becomes more distinct. This can be explained since the channel matrix $\boldsymbol{H}$ here is Gaussian with i.i.d. entries. Such matrices are known to asymptotically preserve the norm of a projected vector [50], thus (32) and (31) become equivalent. To avoid cluttering, we only present the results for $L_{\mathrm{C}} = 4$. Comparison between iterative methods and their non-iterative counterparts indicate that iteratively updating improves accuracy of decoders, while the improvement is not significant.

We next use the objective (32) to design a codebook. After computing distance matrix $\boldsymbol{R}$ in (40), we use the PCA algorithm to reduce the dimensions of the original codewords, and generate candidate codewords $\widetilde{\boldsymbol{p}} \in \mathbb{R}^{L_{\mathrm{D}}}$. The intrinsic dimension of the codewords $\boldsymbol{p}_k$ is estimated as $L_{\mathrm{D}} = 7$ here. Given $N_b = 2^1, 2^3, 2^5$, the k-means method is applied to cluster the candidates $\widetilde{\boldsymbol{p}}$ into N_b classes. The candidate that is closest to the class center is selected as the final codeword. With these final codewords, we test the BER of the 'NonIter + ML' decoder (24) and depict the results in Fig. 11. For comparison, we also test the original codebook which contains $N_b = 2^6$ codewords. As expected, as N_b grows, thus more different messages are conveyed, the overall BER performance is degraded. It is noted that while using smaller N_b values decreases the BER as well as the decoding complexity, it also reduces the data rate, as less bits are conveyed in each symbol.

Finally, we evaluate the impact of the codebook design on radar performance, in comparison with original codebooks that have $N_b = 2^6$ and $N_b = 70$ codewords, respectively. In particular, we consider range-Doppler reconstruction and angle estimate of targets being observed, using hit rate and the root mean squared error (RMSE) as performance metrics, respectively. A hit is proclaimed if the range-Doppler parameter of a scattering point is successfully recovered. The RMSE of the target angle is defined as $\sqrt{\mathrm{E}[(\vartheta_s - \hat{\vartheta}_s)^2]}$, where ϑ_s and $\hat{\vartheta}_s$ denote true angle and estimated one for the s-th target, respectively. The number of radar pulses is set to $N = 32$ and is directed to $\theta = 0$. There are $S = 4$ radar targets inside the beam $\vartheta_s \in \Theta := \theta + [-\frac{\pi}{2L_{\mathrm{R}}}, \frac{\pi}{2L_{\mathrm{R}}}]$ with scattering intensities set to 1. The numerical performance is averaged over 100 Monte Carlo trials. In each trial, the range-Doppler parameters of every target are randomly chosen from the grid points (grid points are explained in [33, Sec. IV]), and the angles are randomly set within the beam Θ. We define the SNR of the radar returns as $1/\kappa^2$, where κ^2 is the variance of the additive i.i.d. zero-mean proper-complex Gaussian noise; see [33, Sec. VII]. The algorithm used for radar signal processing is detailed in [33, Algorithm 1], where Lasso is

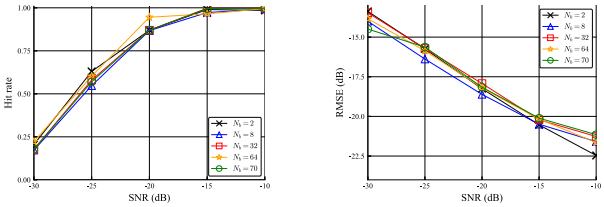

(a) Range-Doppler (b) Angle

Fig. 12. Range-Doppler and angle estimation performance versus SNR.

applied to solve the compressed sensing problem. The resultant range-Doppler reconstruction hit rates and angle estimation performance with the aforementioned codebooks are depicted in Figs. 12 a and 12 b, respectively. Observing these two figures, we note that decreasing the codebook size has only a minimal effect on the range-Doppler and angle estimates of radar targets. This indicates that the proposed codebook reduction method can be used to facilitate the decoding complexity by limiting the number of codewords at the cost of $\log_2 N_b$ less bits conveyed in each symbol with hardly any impact on estimation performance of radar targets.

D. Effect of Imbalanced Codewords on Radar Performance

Finally, we recall that for equiprobable codewords, MAJoRCom implements CAESAR as its radar subsystem, whose performance is analyzed in [33]. As discussed in Subsection V-C, when the codewords are not equiprobable, the radar performance is affected. To evaluate the influence of non-equiprobable codewords on radar performance, we next evaluate the range-Doppler reconstruction performance for two extreme cases: One uses random and independent codewords uniformly distributed over the codebook in each pulse, denoted '- Random,' thus effectively implementing CAESAR; The other transmits the same codewords repeatedly in all pulses, denoted by '- Same'. The remaining simulation settings are the same as those used in our codebook design study in Subsection V-C. We assume that S radar targets correspond to S_D Doppler bins. Here, S_D could be any integer between 1 and S, relying on the realization of the target range-Doppler values. As in the study presented in Fig. 11, we use the hit rates in range-Doppler recovery and sole Doppler recovery as performance metrics, denoted by 'RD' and 'D,' respectively. The range-Doppler recovery method is the same as that used in Subsection V-C. Recall that when the same codewords are repeatedly used, the sensing matrix corresponding to a specific Doppler bin becomes rank deficient. It requires future investigation to propose sparse recovery methods dedicated for the rank deficient case [52], [53]. However, as our purpose is to demonstrate that Doppler recovery is still feasible when MAJoRCom repeatedly uses the same codewords, here we simply extend the traditional Lasso method for sole Doppler reconstruction without rigorous analysis. Particularly in Doppler recovery, the intensity estimates obtained by the Lasso method are divided into groups by their Doppler grid points, and are summed up as the intensity estimates corresponding to the Doppler bins. Then, the S_D Doppler bins with maximum intensities are identified as the Doppler estimates.

The hit rate results are presented in Fig. 13. As expected, using diverse frequency-spatial patterns allows MAJoRCom to achieve improved radar performance compared to using the same pattern repeatedly, i.e., transmitting the same codeword in each pulse. This stems from the fact that the latter transmits only a small portion of the available frequencies, which are not enough for reconstructing the range parameters of radar targets. However, the Doppler recovery ability of both patterns are similar. These results indicate that even in the extreme case that the same codeword is transmitted in all pulses, MAJoRCom is still capable of accurately retrieving some of the target parameters, such as Doppler recovery.

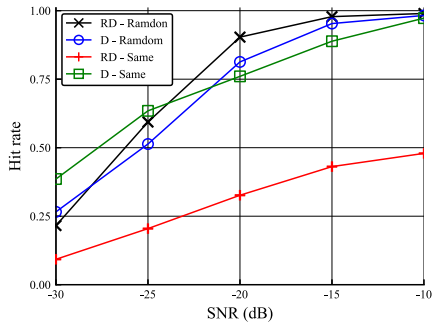

Fig. 13. Hit rates of range-Doppler recovery (denoted 'RD') and Doppler recovery (denoted 'D') using random frequency-spatial patterns (denoted 'Random') and the same pattern (denoted 'Same').

VI. Conclusion

In this paper, we proposed MAJoRCom—a DFRC system which combines frequency and spatial agility. MAJoRCom exploits an inherent randomness in the radar scheme to convey information to a remote receiver using index modulation. In particular, the ability of MAJoRCom to convey digital messages is a natural byproduct of its radar system, and thus does not induce any coexistence and mutual interference issues, unlike most previously proposed DFRC methods. The achievable rate of the proposed communications technique was shown to be comparable to that obtained with dedicated communication waveforms without interfering with the radar functionality. To handle the increased decoding complexity of this scheme, a low complexity receiver and codebook design approach were proposed. Simulation results demonstrate that MAJoRCom exhibits excellent communication performance, and that the proposed low complexity techniques allow to efficiently balance computational burden and communication reliability.

Appendix
Proof of Proposition 2

The symmetry and zero main diagonal of $\boldsymbol{R}$ follow directly from its definition (40). We thus only prove that each row of $\boldsymbol{R}$ is a permutation of its first row.

For each codeword i, there exists an $L_{\mathrm{R}} \times L_{\mathrm{R}}$ permutation matrix $\boldsymbol{\Sigma}_i$ such that $\boldsymbol{\Sigma}_i \boldsymbol{p}_k^{(0)} = \boldsymbol{p}_k^{(i)}$, $k = 0, \ldots, K-1$. This permutation matrix is not unique: two permutations $\boldsymbol{\Sigma}$, $\tilde{\boldsymbol{\Sigma}}$ induce the same codeword (i.e., $\boldsymbol{\Sigma}\boldsymbol{p}_k^{(0)} = \tilde{\boldsymbol{\Sigma}}\boldsymbol{p}_k^{(0)}$ for all k) if and only if $\boldsymbol{\Sigma}^{-1}\tilde{\boldsymbol{\Sigma}}\boldsymbol{p}_k^{(0)} = \boldsymbol{p}_k^{(0)}$, for all k. For convenience, denote by $\mathcal{G}$ the set of all permutation matrices that fix $\boldsymbol{p}_k^{(0)}$ for all k. Choose for each i a permutation matrix $\boldsymbol{\Sigma}_i$ inducing codeword i. The i-th

row of $\boldsymbol{R}$ consists of elements

$$[\boldsymbol{R}]_{i,j} = \sum_{k=0}^{K-1} \left\| \boldsymbol{\Sigma}_i \boldsymbol{p}_k^{(0)} - \boldsymbol{\Sigma}_j \boldsymbol{p}_k^{(0)} \right\|^2. \tag{43}$$

Since permutation matrices are orthogonal, this is equal to

$$\sum_{k=0}^{K-1} \left\| \boldsymbol{p}_k^{(0)} - \boldsymbol{\Sigma}_i^{-1} \boldsymbol{\Sigma}_j \boldsymbol{p}_k^{(0)} \right\|^2. \tag{44}$$

Denote by code_j^i the codeword induced by $\boldsymbol{\Sigma}_i^{-1}\boldsymbol{\Sigma}_j$. Then,

$$[\boldsymbol{R}]_{i,j} = \sum_{k=0}^{K-1} \left\| \boldsymbol{p}_k^{(0)} - \boldsymbol{p}_k^{(\text{code}_j^i)} \right\|^2. \tag{45}$$

For $j \neq j'$, we note that $\boldsymbol{\Sigma}_i^{-1}\boldsymbol{\Sigma}_j$ and $\boldsymbol{\Sigma}_i^{-1}\boldsymbol{\Sigma}_{j'}$ induce different codewords since

$$(\boldsymbol{\Sigma}_i^{-1}\boldsymbol{\Sigma}_j)^{-1}\boldsymbol{\Sigma}_i^{-1}\boldsymbol{\Sigma}_{j'} = \boldsymbol{\Sigma}_j^{-1}\boldsymbol{\Sigma}_{j'} \notin \mathcal{G}. \tag{46}$$

Thus, as j runs through all the codewords, both code_j^0 and code_j^i run through all the codewords. By (45) this implies that the i-th row of $\boldsymbol{R}$ is a permutation of the first row of $\boldsymbol{R}$. ■

ACKNOWLEDGMENT

The authors would like to thank Mr. Dingyou Ma and Mr. Xiang Liu for their fruit discussions on this manuscript.

REFERENCES

[1] T. Huang, X. Xu, Y. Liu, N. Shlezinger, and Y. C. Eldar, "A dual-function radar communication system using index modulation," in *Proc. IEEE 20th Int. Workshop Signal Process. Advances Wireless Commun.*, Jul. 2019, pp. 1–5.

[2] T. Huang, N. Shlezinger, X. Xu, D. Ma, Y. Liu, and Y. C. Eldar, "Complexity reduction methods for index modulation based dual-function radar communication systems," in *Proc. IEEE Int. Conf. Acoustics, Speech, Signal Proc.*, May 2020, pp. 5080–8084.

[3] A. Hassanien, M. G. Amin, Y. D. Zhang, and F. Ahmad, "Signaling strategies for dual-function radar communications: An overview," *IEEE Aerosp. Electron. Syst. Mag.*, vol. 31, no. 10, pp. 36–45, Oct. 2016.

[4] B. Paul, A. R. Chiriyath, and D. W. Bliss, "Survey of RF communications and sensing convergence research," *IEEE Access*, vol. 5, pp. 252–270, 2017.

[5] K. V. Mishra, V. Koivunen, B. Ottersten, and S. A. Vorobyov, "Towards millimeter wave joint radar-communications: A signal processing perspective," *IEEE Trans. Signal Process.*, vol. 36, no. 5, pp. 100–114, 2019.

[6] D. Ma, N. Shlezinger, T. Huang, Y. Liu, and Y. C. Eldar, "Joint radar-communications strategies for autonomous vehicles," *IEEE Signal Process. Mag.*, to be published.

[7] L. Zheng, M. Lops, Y. C. Eldar, and X. Wang, "Radar and communication coexistence: An overview: A review of recent methods," *IEEE Signal Process. Mag.*, vol. 36, no. 5, pp. 85–99, Sep. 2019.

[8] G. C. Tavik *et al.*, "The advanced multifunction RF concept," *IEEE Trans. Microw. Theory Tech.*, vol. 53, no. 3, pp. 1009–1020, Mar. 2005.

[9] Y. Liu, G. Liao, J. Xu, Z. Yang, and Y. Zhang, "Adaptive OFDM integrated radar and communications waveform design based on information theory," *IEEE Commun. Lett.*, vol. 21, no. 10, pp. 2174–2177, Oct. 2017.

[10] L. Zheng, M. Lops, X. Wang, and E. Grossi, "Joint design of overlaid communication systems and pulsed radars," *IEEE Trans. Signal Process.*, vol. 66, no. 1, pp. 139–154, Jan. 2018.

[11] X. Wang, A. Hassanien, and M. G. Amin, "Dual-function MIMO radar communications system design via sparse array optimization," *IEEE Trans. Aerosp. Electron. Syst.*, vol. 55, no. 3, pp. 1213–1226, Jun. 2019.

[12] C. Sturm and W. Wiesbeck, "Waveform design and signal processing aspects for fusion of wireless communications and radar sensing," *Proc. IEEE*, vol. 99, no. 7, pp. 1236–1259, Jul. 2011.

[13] A. Hassanien, M. G. Amin, Y. D. Zhang, and F. Ahmad, "Phase-modulation based dual-function radar-communications," *IET Radar, Sonar Navigation*, vol. 10, no. 8, pp. 1411–1421, 2016.

[14] F. Liu, L. Zhou, C. Masouros, A. Li, W. Luo, and A. Petropulu, "Towards dual-functional radar-communication systems: Optimal waveform design," *IEEE Trans. Signal Process.*, vol. 66, no. 16, pp. 4264–4279, 2018.

[15] F. Liu, C. Masouros, A. Li, H. Sun, and L. Hanzo, "MU-MIMO communications with MIMO radar: From co-existence to joint transmission," *IEEE Trans. Wireless Commun.*, vol. 17, no. 4, pp. 2755–2770, Apr. 2018.

[16] J. A. Mahal, A. Khawar, A. Abdelhadi, and T. C. Clancy, "Spectral coexistence of MIMO radar and MIMO cellular system," *IEEE Trans. Aerosp. Electron. Syst.*, vol. 53, no. 2, pp. 655–668, Apr. 2017.

[17] F. Liu, C. Masouros, A. Li, T. Ratnarajah, and J. Zhou, "MIMO radar and cellular coexistence: A power-efficient approach enabled by interference exploitation," *IEEE Trans. Signal Process.*, vol. 66, no. 14, pp. 3681–3695, Jul. 2018.

[18] N. Nartasilpa, A. Salim, D. Tuninetti, and N. Devroye, "Communications system performance and design in the presence of radar interference," *IEEE Trans. Commun.*, vol. 66, no. 9, pp. 4170–4185, Sep. 2018.

[19] M. Bică and V. Koivunen, "Multicarrier radar-communications waveform design for RF convergence and coexistence," in *Proc. IEEE Int. Conf. Acoust., Speech Signal Process.*, May 2019, pp. 7780–7784.

[20] P. M. McCormick, S. D. Blunt, and J. G. Metcalf, "Simultaneous radar and communications emissions from a common aperture, part I: Theory," in *Proc. IEEE RadarConf*, May 2017, pp. 1685–1690.

[21] F. Liu, L. Zhou, C. Masouros, A. Li, W. Luo, and A. Petropulu, "Toward dual-functional radar-communication systems: Optimal waveform design," *IEEE Trans. Signal Process.*, vol. 66, no. 16, pp. 4264–4279, Aug. 2018.

[22] X. Liu, T. Huang, Y. Liu, J. Zhou, N. Shelzinger, and Y. C. Eldar, "Joint transmit beamforming for multiuser MIMO communications and radar," 2019, *arXiv:1912.03420*.

[23] D. Ma, T. Huang, Y. Liu, and X. Wang, "A novel joint radar and communication system based on randomized partition of antenna array," in *Proc. IEEE Int. Conf. Acoust., Speech Signal Process.*, Apr. 2018, pp. 3335–3339.

[24] J. Wang, S. Jia, and J. Song, "Generalised spatial modulation system with multiple active transmit antennas and low complexity detection scheme," *IEEE Trans. Wireless Commun.*, vol. 11, no. 4, pp. 1605–1615, Apr. 2012.

[25] M. Di Renzo, H. Haas, A. Ghrayeb, S. Sugiura, and L. Hanzo, "Spatial modulation for generalized MIMO: Challenges, opportunities, and implementation," *Proc. IEEE*, vol. 102, no. 1, pp. 56–103, Jan. 2014.

[26] A. R. Chiriyath, B. Paul, and D. W. Bliss, "Radar-communications convergence: Coexistence, cooperation, and co-design," *IEEE Trans. Cogn. Commun. Netw.*, vol. 3, no. 1, pp. 1–12, Mar. 2017.

[27] J. Qian, M. Lops, L. Zheng, X. Wang, and Z. He, "Joint system design for coexistence of MIMO radar and MIMO communication," *IEEE Trans. Signal Process.*, vol. 66, no. 13, pp. 3504–3519, Jul. 2018.

[28] D. Gaglione *et al.*, "Waveform design for communicating radar systems using fractional Fourier transform," *Digit. Signal Process.*, vol. 80, pp. 57–69, 2018.

[29] P. Striano, C. V. Ilioudis, C. Clemente, and J. J. Soraghan, "Fractional Fourier transform based joint radar communication system for multi-user automotive applications," in *Proc. IEEE Radar Conf. (RadarConf)*, Apr. 2019, pp. 1–6.

[30] D. Cohen, D. Cohen, Y. C. Eldar, and A. M. Haimovich, "SUMMeR: Sub-Nyquist MIMO radar," *IEEE Trans. Signal Process.*, vol. 66, no. 16, pp. 4315–4330, Aug. 2018.

[31] A. Hassanien, M. G. Amin, Y. D. Zhang, and F. Ahmad, "Dual-function radar-communications: Information embedding using sidelobe control and waveform diversity," *IEEE Trans. Signal Process.*, vol. 64, no. 8, pp. 2168–2181, Apr. 2016.

[32] A. Hassanien, B. Himed, and B. D. Rigling, "A dual-function MIMO radar-communications system using frequency-hopping waveforms," in *Proc. IEEE Radar Conf*, May 2017, pp. 1721–1725.

[33] T. Huang, N. Shlezinger, X. Xu, D. Ma, Y. Liu, and Y. C. Eldar, "Multi-carrier agile phased array radar," 2019, *arXiv:1906.06289*.

[34] S. R. J. Axelsson, "Analysis of random step frequency radar and comparison with experiments," *IEEE Trans. Geosci. Remote Sens.*, vol. 45, no. 4, pp. 890–904, Apr. 2007.

[35] E. Basar, "Index modulation techniques for 5G wireless networks," *IEEE Commun. Mag.*, vol. 54, no. 7, pp. 168–175, Jul. 2016.

[36] N. Ishikawa, S. Sugiura, and L. Hanzo, "50 years of permutation, spatial and index modulation: From classic RF to visible light communications and data storage," *IEEE Commun. Surv. Tut.*, vol. 20, no. 3, pp. 1905–1938, Jul.–Sep. 2018.
[37] E. Basar, "OFDM with index modulation using coordinate interleaving," *IEEE Wireless Commun. Lett.*, vol. 4, no. 4, pp. 381–384, Aug. 2015.
[38] M. Wen, B. Ye, E. Basar, Q. Li, and F. Ji, "Enhanced orthogonal frequency division multiplexing with index modulation," *IEEE Trans. Wireless Commun.*, vol. 16, no. 7, pp. 4786–4801, Jul. 2017.
[39] S. U. Pillai, *Array Signal Processing*, C. S. Burrus, Ed. Berlin, Germany: Springer, 1989.
[40] D. Slepian, "Permutation modulation," *Proc. IEEE*, vol. 53, no. 3, pp. 228–236, Mar. 1965.
[41] T. Datta, H. S. Eshwaraiah, and A. Chockalingam, "Generalized space-and-frequency index modulation," *IEEE Trans. Veh. Technol.*, vol. 65, no. 7, pp. 4911–4924, Jul. 2016.
[42] E. Brookner, "MIMO radar demystified and where it makes sense to use," in *Proc. IEEE Int. Symp. Phased Array Syst. Technol.*, Oct. 2013, pp. 399–407.
[43] S. Sodagari, A. Khawar, T. C. Clancy, and R. McGwier, "A projection based approach for radar and telecommunication systems coexistence," in *Proc. IEEE GLOBECOM*, Dec. 2012, pp. 5010–5014.
[44] F. Xi, S. Chen, and Z. Liu, "Quadrature compressive sampling for radar signals," *IEEE Trans. Signal Process.*, vol. 62, no. 11, pp. 2787–2802, Jun. 2014.
[45] S. S. Ioushua, O. Yair, D. Cohen, and Y. C. Eldar, "CaSCADE: Compressed carrier and DOA estimation," *IEEE Trans. Signal Process.*, vol. 65, no. 10, pp. 2645–2658, May 2017.
[46] M. Wen, X. Cheng, M. Ma, B. Jiao, and H. V. Poor, "On the achievable rate of OFDM with index modulation," *IEEE Trans. Signal Process.*, vol. 64, no. 8, pp. 1919–1932, Apr. 2016.
[47] T. M. Cover and J. A. Thomas, *Elements of Information Theory*. Hoboken, NJ, USA: Wiley, 2006.
[48] M. F. Huber, T. Bailey, H. Durrant-Whyte, and U. D. Hanebeck, "On entropy approximation for gaussian mixture random vectors," in *Proc. IEEE MFI*, Aug. 2008, pp. 181–188.
[49] A. Goldsmith, *Wireless Communications*. New York, NY, USA: Cambridge Univ. Press, 2005.
[50] Y. C. Eldar and G. Kutyniok, *Compressed Sensing: Theory and Applications*. Cambridge, U.K.: Cambridge Univ. Press, 2012.
[51] L. van der Maaten, E. Postma, and J. van den Herik, "Dimensionality reduction: A comparative review," Tilburg Univ., Tilburg, The Netherlands, Tech. Rep. TiCC-TR 2009-005, 2009.
[52] E. Elhamifar and R. Vidal, "Block-sparse recovery via convex optimization," *IEEE Trans. Signal Process.*, vol. 60, no. 8, pp. 4094–4107, Aug. 2012.
[53] L. Wang, T. Huang, and Y. Liu, "Theoretical analysis for extended target recovery in randomized stepped frequency radars," 2019, *arXiv:1908.02929*.

Tianyao Huang received the B.S. degree in 2009 in telecommunication engineering from the Harbin Institute of Technology, Heilongjiang, China, and the Ph.D degree in 2014 in electronics engineering from the Tsinghua University, Beijing, China, respectively. From 2014 to 2017, he was a radar Researcher in Aviation Industry Corporation of China (AVIC). Since July 2017, he has joined Intelligent Sensing Lab, Department of Electronic Engineering, Tsinghua University, as an Assistant Professor. His current research interests include signal processing, compressed sensing, and joint radar communications system design.

Nir Shlezinger received his B.Sc., M.Sc., and Ph.D. degrees in 2011, 2013, and 2017, respectively, from Ben-Gurion University, Israel, all in electrical and computer engineering. From 2017 to 2019, he was a postdoctoral researcher in the Technion Israel Institute of Technology and is currently a postdoctoral researcher in the Signal Acquisition Modeling, Processing, and Learning Lab,Weizmann Institute of Science. From 2009 to 2013, he worked as a research and development engineer at Yitran Communications. His research interests include communications, information theory, signal processing, and machine learning.

Xingyu Xu received the B.S. degree in the Department of electronic engineering at Tsinghua University, Beijing, China, in 2019, and is now pursuing the Ph.D. degree in the same department. His research interests include topological and statistical data analysis.

Yimin Liu (Member, IEEE) received the B.S. and Ph.D. degrees (both with honors) in electronics engineering from the Tsinghua University, China, in 2004 and 2009, respectively. From 2004, he was with the Intelligence Sensing Lab (ISL), Department of Electronic Engineering, Tsinghua University. He is currently an Associate Professor with Tsinghua, where his field of activity is to study new concept radar and other microwave sensing technologies. His current research interests include radar theory, statistic signal processing, compressive sensing and their applications in radar, spectrum sensing and intelligent transportation systems.

Yonina C. Eldar (Fellow, IEEE) received the B.Sc. degree in physics and the B.Sc. degree in electrical engineering from Tel-Aviv University, Tel-Aviv, Israel, 1995, 1996, respectively, and the Ph.D. degree in electrical engineering and computer science from the Massachusetts Institute of Technology (MIT), Cambridge, MA, USA, in 2002. She is currently a Professor with the Department of Mathematics and Computer Science, Weizmann Institute of Science, Rehovot, Israel. She was previously a Professor with the Department of Electrical Engineering, the Technion, where she held the Edwards Chair in Engineering. She is also a Visiting Professor with MIT, a Visiting Scientist with the Broad Institute, and an Adjunct Professor with Duke University, and was a Visiting Professor with Stanford. She is a member of the Israel Academy of Sciences and Humanities (elected 2017), and a EURASIP Fellow. She is also an author of the book *Sampling Theory: Beyond Bandlimited Systems* and co-author of four other books published by Cambridge University Press. Her research interests include statistical signal processing, sampling theory and compressed sensing, learning and optimization methods, and their applications to biology, medical imaging and optics. Dr. Eldar has received many awards for excellence in research and teaching, including the IEEE Signal Processing Society Technical Achievement Award (2013), the IEEE/AESS Fred Nathanson Memorial Radar Award (2014), and the IEEE Kiyo Tomiyasu Award (2016). She was a Horev Fellow of the Leaders in Science and Technology program with the Technion and an Alon Fellow. She received the Michael Bruno Memorial Award from the Rothschild Foundation, the Weizmann Prize for Exact Sciences, the Wolf Foundation Krill Prize for Excellence in Scientific Research, the Henry Taub Prize for Excellence in Research (twice), the Hershel Rich Innovation Award (three times), the Award for Women with Distinguished Contributions, the Andre and Bella Meyer Lectureship, the Career Development Chair with the Technion, the Murieland David Jacknow Award for Excellence in Teaching, and the Technions Award for Excellence in Teaching (two times). She received several best paper awards and best demo awards together with her research students and colleagues including the SIAM outstanding Paper Prize, the UFFC Outstanding Paper Award, the Signal Processing Society Best Paper Award and the IET Circuits, Devices and Systems Premium Award, was selected as one of the 50 most influential women in Israel and in Asia, and is a highly cited researcher. She was a member of the Young Israel Academy of Science and Humanities and the Israel Committee for Higher Education. She is the Editor-in-Chief of Foundations and Trends in Signal Processing, a member of the IEEE Sensor Array and Multichannel Technical Committee and serves on several other IEEE committees. In the past, she was a Signal Processing Society Distinguished Lecturer, member of the IEEE Signal Processing Theory and Methods and Bio Imaging Signal Processing technical committees, and served as an Associate Editor for the IEEE TRANSACTIONS ON SIGNAL PROCESSING, the *EURASIP Journal of Signal Processing*, the *SIAM Journal on Matrix Analysis and Applications*, and the *SIAM Journal on Imaging Sciences*. She was Co-Chair and Technical Co-Chair of several international conferences and workshops.